

Hegranesþing on Hegranes: Geophysical Prospection
Interim Report 2013 – 2015



Brian N. Damiata
John Steinberg
John Schoenfelder
Douglas J. Bolender

2/27/2016

Photo on front page – John Steinberg and Brian Damiata using the GF Instruments' CMD conductivity meter at Hegransþing.



Brian N. Damiata, John Steinberg, John Schoenfelder, Douglas J. Bolender
Byggðasafn Skagfirðinga/Fiske Center for Archaeological Research, UMass Boston
BSK 2016-164 / SCASS 2016-3

2016

ACKNOWLEDGEMENTS

We thank the owner of Garður, Jón Sigurjónsson, for his kind permission and support of our work at Hegranesþing. John Steinberg, Allison Carlton, and Colin Lenfest assisted in the survey, which was directed by Brian Damiata. John Schoenfelder oversaw the mapping and kite photography. Douglas Bolender used those images to create the georeferenced images and other illustrations.

The Hegranesþing geophysical survey is part of a larger survey of Hegranes. General permits for the survey of Hegranes and associated excavations were granted by The Cultural Heritage Agency of Iceland (MÍ201506-0056, MÍ201506-0058, & MÍ201506-0059). The work was supported by the US National Science Foundation (PLR # 1242829, 1345066, 1417772 & 1523025) in a joint project of the Skagafjörður Heritage Museum and UMass Boston. The Icelandic Archaeology Fund also supplied significant support for the project. We are grateful to the Skagafjörður Commune for their ongoing and invaluable support. Any opinions, findings, conclusions, or recommendations expressed in this material are those of the authors and do not necessarily reflect the views of the individuals and institutions who support this work.

SKAGAFJÖRÐUR HERITAGE MUSEUM

The Skagafjörður Heritage Museum is a center for research on local history and cultural heritage in the Skagafjörður region, North Iceland. It is affiliated with the National Museum of Iceland and its main exhibition at the old turf farm of Glaumbær is one of the most visited national heritage tourist attractions. The Archaeological Department of the museum was established in 2003 and engages in contract and research driven archaeology both within and outside the region. The core long-term research programs center on fundamental issues surrounding the settlement and early medieval church history of Skagafjörður and the North-Atlantic region with a focus on developing methodological and theoretical approaches to the geography of early Christian cemeteries. The department is involved in multifaceted interdisciplinary collaboration with Icelandic and international institutions and specialists. Its research portfolio includes bioarchaeology, early metal production, settlement studies, as well as the methodological aspects of archaeological surveying.

FISKE CENTER FOR ARCHAEOLOGICAL RESEARCH

The Andrew Fiske Memorial Center for Archaeological Research at the University of Massachusetts Boston was established in 1999 through the generosity of the late Alice Fiske and her family as a living memorial to her late husband Andrew. As an international leader in interdisciplinary research, the Fiske Center promotes a vision of archaeology as a multi-faceted, theoretically rigorous field that integrates a variety of analytical perspectives into its studies of the cultural and biological dimensions of colonization, urbanization, and industrialization that have occurred over the past one thousand years in the Americas and the Atlantic World. As part of a public university, the Fiske Center maintains a program of local archaeology with a special emphasis on research that meets the needs of cities, towns, and Tribal Nations in New England and the greater Northeast. The Fiske Center also seeks to understand the local as part of a broader Atlantic World.

SKAGAFJÖRÐUR CHURCH AND SETTLEMENT SURVEY

The Skagafjörður Church and Settlement Survey (SCASS) seeks to determine if the settlement pattern of the 9th-century colonization of Iceland affected the development of the religious and economic institutions that dominated the 14th century. The research builds on the combined methods and results of two projects. One has focused on Viking Age settlement patterns. The other has been investigating the changing geography of early Christian cemeteries. Together, the research seeks to understand the connections between the Viking settlement hierarchy and the Christian consolidation.

Contents

ACKNOWLEDGEMENTS	ii
SKAGAFJÖRÐUR HERITAGE MUSEUM	iii
FISKE CENTER FOR ARCHAEOLOGICAL RESEARCH	iv
SKAGAFJÖRÐUR CHURCH AND SETTLEMENT SURVEY	v
1.0 INTRODUCTION	1
2.0 LAND SURVEYING AND ESTABLISHMENT OF GRIDS	1
3.0 GEOPHYSICAL METHODOLOGIES	3
3.1 Site Conditions and Geophysical Targets	3
3.2 Frequency-Domain Electromagnetic Surveying	4
3.2.1 Equipment and Field Procedures	4
3.2.2 Data Processing.....	5
3.2.3 Results.....	5
3.3 Time-Domain Reflectometry	15
3.3.1 Equipment and Field Procedures	15
3.3.2 Data Processing.....	15
3.3.3 Results.....	15
3.4 Ground-Penetrating Radar.....	16
3.4.1 Equipment and Field Procedures	17
3.4.2 Data Processing.....	17
3.4.3 Results.....	18
4.0 SUMMARY AND CONCLUSIONS	23
5.0 REFERENCES	24
APPENDIX A – BASIC PRINCIPLES OF FREQUENCY-DOMAIN ELECTROMAGNETICS	25
APPENDIX B – BASIC PRINCIPLES OF GROUND-PENETRATING RADAR.....	27
APPENDIX C – PLOT OF FDEM DATA	29
APPENDIX D – ANNOTATED RADARGRAMS	38

List of Figures

Figure 1. Location of geophysical surveys conducted in 2013 and 2015 superimposed on kite-based photo-mosaic of southern part of Hegranesþing.....	2
Figure 2. Using the CMD Explorer with the boom oriented perpendicularly to the direction of transects.....	5
Figure 3. Results of FDEM survey conducted in 2013. Upper Left: Optical topographic image of area that was obtained by kite-based photography. Upper Right: Hill-shaded topographic image. Lower Left: Gray-shaded plot of apparent ground conductivity data (sensor 2, dipole length = 2.82 m). Lower Right: Gray-shaded plot of corresponding in-phase.	7
Figure 4. Left: Color-contour plot of apparent ground conductivity data (sensor 2, dipole length = 2.82 m) from survey conducted in 2013. Right: Gray-shaded plot.....	8
Figure 5. Left: Color-contour plot of in-phase data (sensor 2, dipole length = 2.82 m) from survey conducted in 2013. Right: Gray-shaded plot.	9
Figure 6. Results of FDEM survey conducted in 2015. Upper Left: Optical topographic image of area that was obtained by kite-based photography. Upper Right: Hill-shaded topographic image. Lower Left: Gray-shaded plot of apparent ground conductivity data (sensor 2, dipole length = 2.82 m). Lower Right: Gray-shaded plot of corresponding in-phase.	10
Figure 7. Left: Color-contour plot of apparent ground conductivity data (sensor 2, dipole length = 2.82 m) from survey conducted in 2015. Right: Gray-shaded plot.....	11
Figure 8. Left: Color-contour plot of in-phase data (sensor 2, dipole length = 2.82 m) from survey conducted in 2015. Right: Gray-shaded plot.	12
Figure 9. Comparison of in-phase data (sensor 2, dipole length = 2.82 m) from survey conducted in 2013. Middle Left: Hill-shaded topographic image. Upper Right: Data plotted based on normal histogram. Middle Right: Data plotted based on equalization histogram. Lower Right: Data plotted based on equalization histogram of the residual after background removal (second-order polynomial trend). Red rectangle and arrows highlight partially exposed archaeological remains (booth and a section of the homefield's boundary wall).	13
Figure 10. Comparison of in-phase data (sensor 2, dipole length = 2.82 m) from survey conducted in 2015. Middle Left: Hill-shaded topographic image. Upper Right: Data plotted based on normal histogram. Middle Right: Data plotted based on equalization histogram. Lower Right: Data plotted based on equalization	

histogram of the residual after background removal (second-order polynomial trend). Red rectangle and arrows highlights partially exposed archaeological remains (booths and a section of the homefield’s boundary wall).....	14
Figure 11. Photograph of the Trase 6050X1 TDR instrumentation.....	16
Figure 12. Photograph of the Mala X3 equipped with a 500 MHz antenna.	18
Figure 13. Overlay depth-slice images from GPR survey conducted in 2013 in the eastern inner part of cemetery at Hegranesþing (see Figure 1 for location). Strong reflections are denoted in red.	19
Figure 14. Interpreted below-ground burials from Table 1superimposed on GPR Slice 27 (102-110 cm bgs – Appendix E), superimposed on Kite Air Photo. Also shown are 2003 and 2009 excavations and burials identified in those excavations (Zoëga, 2009).....	21
Figure 15 Close up of interpreted below-ground burials from Table 1superimposed on GPR Slice 27 (102-110 cm bgs – Appendix E), superimposed on FDEM in-phase sensor 2 (Figure 8). Also shown are 2003 and 2009 excavations and Burials identified in those excavations (Zoëga, 2009).	22
Figure A1. Schematic diagram illustrating the principles of FDEM.	26
Figure B1. Schematic diagram illustrating the principles of GPR.....	28
Figure C1. Left: Color-contour plot of apparent ground conductivity data (sensor 1, dipole length = 1.48 m) from survey conducted in 2013. Right: Gray-shaded plot.....	30
Figure C2. Color-contour plot of in-phase data (sensor 1, dipole length = 1.48 m) from survey conducted in 2013. Right: Gray-shaded plot.	31
Figure C3. Left: Color-contour plot of apparent ground conductivity data (sensor 3, dipole length = 4.49 m) from survey conducted in 2013. Right: Gray-shaded plot.....	32
Figure C4. Color-contour plot of in-phase data (sensor 3, dipole length = 4.49 m) from survey conducted in 2013. Right: Gray-shaded plot.	33
Figure C5. Plots of apparent ground conductivity data and (sensor 1, dipole length = 1.48 m) from survey conducted in 2015.	34
Figure C6. Color Color-contour plot of in-phase data (sensor 1, dipole length = 1.48 m) from survey conducted in 2015. Right: Gray-shaded plot.	35

Figure C7. Plots Left: Color-contour plot of apparent ground conductivity data (sensor 3, dipole length = 4.49 m) from survey conducted in 2015. Right: Gray-shaded plot..	36
Figure C8. Color-contour plot of in-phase data (sensor 3, dipole length = 4.49 m) from survey conducted in 2015. Right: Gray-shaded plot.	37
Figure D1. Annotated radargrams for profiles 5246 (478645.0E) through 5265 (478648.8E).	39
Figure D2. Annotated radargrams for profiles 5266 (478649.0E) through 5285 (478652.8E).	40
Figure D3. Annotated radargrams for profiles 5286 (478653.0E) through 5305 (478656.8E).	41
Figure D4. Annotated radargrams for profiles 5306 (478657.0E) through 5316 (478659.0E).	42

List of Tables

Table 1. Interpreted below-ground burials associated with GPR reflections; see Appendix D for annotated radargrams.	20
--	----

1.0 INTRODUCTION

Geophysical surveys were conducted at Hegranesþing on Hegranes during the summers of 2013 and 2015 (Figure 1). The work in 2013 was a preliminary part of The Skagafjörður Church and Settlement Survey (SCASS) project to investigate and analyze the use of geophysical methods to locate and image early Christian churchyards in Iceland (Testing Geophysical Prospection and Mapping Methods for Early Christian Cemeteries in Iceland, funded by the United States National Science Foundation, EAGER #1345066). The specific objective of the 2013 project was to develop a geophysical protocol to locate churchyards and map their graves. Hegranesþing—the site of the local assembly during Viking/early medieval times—was selected as one of five sites to be investigated because the geophysical results could be easily evaluated given that a surface expression of a churchyard still exists (Friðriksson *et al.* 2004), and previous excavations had confirmed the presence of well-preserved skeletal remains within the churchyard’s confines (Zoëga 2009). Geophysical surveys were performed over the churchyard proper and its near vicinity.

The work in 2015 was part of the basic SCASS project (described in the front matter), and was implemented to identify traces of settlement or other churches or churchyards at the northern area of the farm of Garður (Hegranesþing). An additional goal was to compare geophysical results to the exposed archaeological remains. Today, this area is in pasture. A visible boundary wall which intersects the visible churchyard wall attests that this area has been a home field probably associated with a farmstead named Litli-Garður (Pálsson 2010; Zoëga 2009). Geophysical surveying was extended beyond the visible churchyard to cover a substantial portion of the pasture, grass field, and boundary wall adjacent to the visible churchyard, as well as the archaeological remains that are associated with the Hegranesþing (Figure 1).

2.0 LAND SURVEYING AND ESTABLISHMENT OF GRIDS

All land-survey data were collected based on the ISN93 coordinate system. Initial set-up points were established using a Trimble GeoXH with a Zepher antenna and by recording hundreds of measurements at a 5-second interval. The GPS data were post-corrected and then averaged to obtain ISN93 coordinates. These points were then used to set up a total station. The original GPS points were re-measured with the total station to ensure

consistency across different total-station set ups. The corner points of the survey area and internal grids at intervals of 50 x 50 meters were flagged using the total station. Additional flags were laid out at intervals of 10 x 10 meters using fiberglass measuring tapes that were stretched between the stations established by the total station. The northern and southern baselines of the entire grid were flagged at 1-m intervals using alternating colors. Additional lines of alternating flags running east to west were laid out 10 meters apart to help guide the surveying.

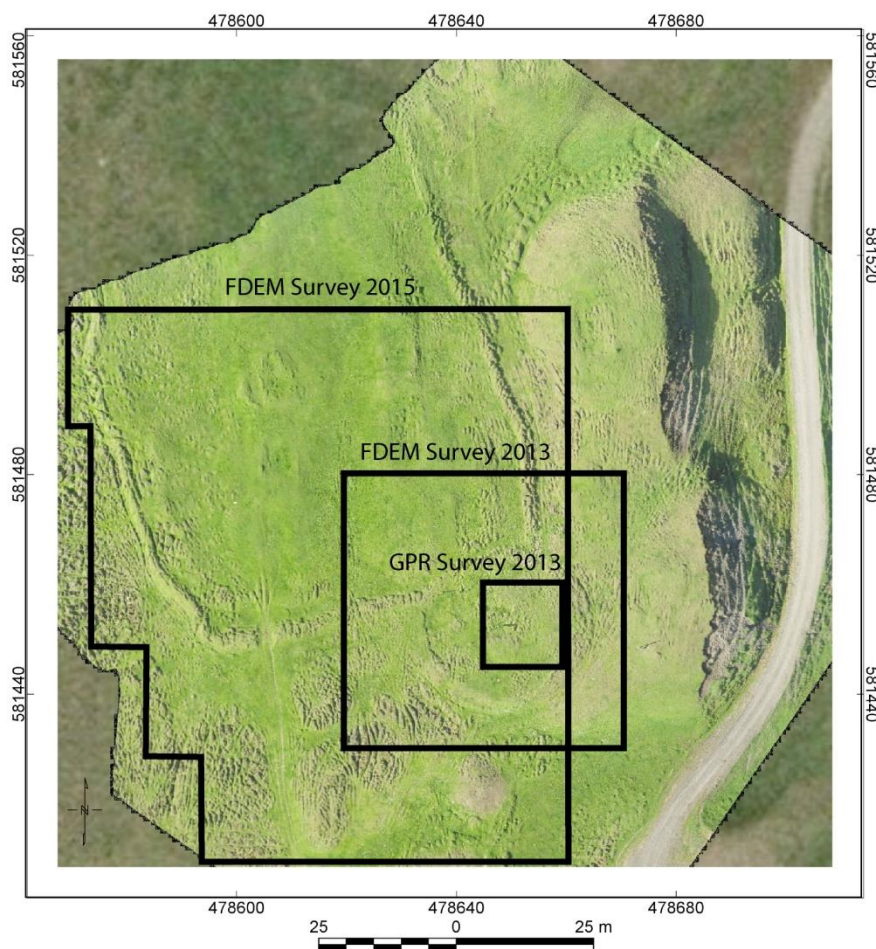


Figure 1. Location of geophysical surveys conducted in 2013 and 2015 superimposed on kite-based photo-mosaic of southern part of Hegranesping.

3.0 GEOPHYSICAL METHODOLOGIES

The use of geophysical methods in support of archaeological investigations is widely established (e.g., Gaffney and Gater 2003; Linford 2006). For the present study, frequency-domain electromagnetics (FDEM), time-domain reflectometry (TDR) and ground-penetrating radar (GPR) were applied over portions of the churchyard and the near vicinity. Summarized below are the geophysical methodologies that were used. Appendices A and B provide general overviews of FDEM and GPR, respectively.

3.1 Site Conditions and Geophysical Targets

The natural stratigraphy of the region consists of soil with intermixed tephra layers, along with gravel layers and lenses of glacial origin. The soil is a brown andosol that derives from aeolian sediments of volcanic origin, but is not the direct product of eruptions (Arnalds et al. 1995; Arnalds 2004, 2008). The andosol is non-cohesive but has an extremely high water-retention capacity (Arnalds 2008). At Hegranesþing, the ground surface is hummocky due to a combination of thufurs (frost heaves) (e.g., Grab 2005) and the remnants of archaeological remains. A limited excavation within the cemetery proper yielded fill layers overlying a gravel deposit below which two well-preserved skeletons were revealed (Zoëga 2009).

There are several potential geophysical targets associated with the Viking Age archaeological remains at Hegranesþing. In general, churchyards consist of a small central church that is surrounded by a cemetery, which is enclosed by a circular wall. The churches are often only 3 x 4 m in size and constructed of wood with stone foundation. The wall is typically between 15 to 30 m in diameter and composed of compacted turf overlying a stone foundation or gravel base. Graves may be found throughout the enclosed cemetery including under the church. Similarly, other archaeological remains (e.g., booths, walls) are expected to consist of compacted turf blocks overlying a stone foundation. In some cases, the turf will be placed directly on the ground or on a prepared surface. From a geophysical perspective, measureable contrasts between stones and soil and between compacted turf and soil are anticipated (i.e., contrast in relative permittivity for GPR and in apparent ground conductivity and in-phase for FDEM).

Graves can be a difficult geophysical target to detect but differential fill, breaks in soil stratigraphy, and the interfaces along the sides and bottom of grave shafts might be detectable

(Bevan 1991; King *et al.* 1993; Conyers 2005, 2006; Jones 2008; Doolittle and Bellantoni 2010). In some instances, the direct detection of skeletal remains is possible (Schultz 2008; Schultz and Martin 2011; Damiata *et al.* 2013). Specifically, the contrast in relative permittivity between well-preserved bones and soil, and to a lesser extent between bones and gravel, may be detectable by GPR.

3.2 Frequency-Domain Electromagnetic Surveying

In 2013, an FDEM survey was conducted over a 50 x 50 m grid, which was primarily intended to investigate the churchyard. In 2015, an expanded reconnaissance survey was conducted over areas to the south, north and west of the churchyard—including most of the homefield. The work was As part of this work was in order to directly compare geophysical results to the exposed archaeological remains (see Figure 1).

3.2.1 Equipment and Field Procedures

The FDEM surveys were conducted using a GF Instruments' CMD Explorer (Figure 2), which operates at 30 kHz over three separate dipole lengths (i.e., a single transmitter [TX] located at one end of the unit and three separate receivers [RX] located at varying distances along the boom). By increasing dipole length, a greater volume and depth of soil can be sensed. When operated in the vertical dipole mode, the dipole lengths of 1.48, 2.82 and 4.49 m provide depths of interrogation of approximately 2.2, 4.2 and 6.7 m (i.e., ~1.5X the dipole length), respectively, relative to the level of the sensors.

For both surveys, the instrument was operated in the vertical dipole mode with the boom carried at hip level. For the survey in 2013, the boom was oriented perpendicularly to the direction of transects, whereas in 2015 it was parallel. Both surveys were conducted unidirectionally in that all data for a given survey were collected by traversing from south to north. Data were collected along contiguous transects that were separated by 0.5 m. The sampling rate was set to 10 Hz (i.e., 10 samples per second), which yielded a spacing between measurements of ~0.06 m while walking at a normal pace. Note that surveying was guided by color-coded PVC flags that were placed every 10 meters along transects separated by 1 m. The true location of measurement was determined by fiducial markers that were placed into the data stream by the operator and assuming linear interpolation between markers. Both quadrature phase (bulk ground conductivity) and in-phase (related to bulk

ground magnetic susceptibility) components were recorded for each of the three dipole lengths (i.e., six simultaneous readings were recorded for each “measurement”), which yielded more than 70,800 and 138,700 readings for each of the two components for each of the three dipole lengths for the surveys in 2013 and 2015, respectively.



Figure 2. Using the CMD Explorer with the boom oriented perpendicularly to the direction of transects.

3.2.2 Data Processing

The raw data were initially corrected to properly adjust for the starting and ending locations of each transect. As a check on quality control, the average spacing of measurements for each fiducial segment along a given transect (i.e., every 10 m) was calculated to ensure the spacing between measurements was approximately 0.07 m or less. The data were then processed using Oasis Montaj mapping software to produce grey-shaded and color-contoured maps. The processed data were also archived into a database for future use.

3.2.3 Results

Figure 3 depicts a comparison between optical/hill-shaded images and gray-shaded plots of the FDEM data for the survey in 2013, which focused on the churchyard. The data from

sensor 2 (dipole length = 2.82 m) was selected because it provides the best qualitative match to the partially visible archaeological remains. Figures 4 and 5 present color plots of the same data. Similarly, Figure 6 depicts gray-shaded plots from sensor 2 for the survey in 2015, which focused on the broader area to the south, west and north of the churchyard, while Figures 7 and 8 are the associated color plots of the data. In addition, plots for the other two sensors for both surveys are provided in Appendix C.

Of specific interest is an area of relatively high apparent ground conductivity and high in-phase that occurs in the northern part of the survey from 2015 (see color-contour plots in Figures 7 and 8) at about E 478610 N 581500. Although the cause for the relatively high values for both components is unknown, the presence of peat ash would be consistent with such values. The anomalies in this area seem to be less well-defined than the potential booths and other structures. If the high values are caused by peat ash this could be the location of Litli-Garður, mentioned in several sources (Pálsson 2010:45) or another unknown early farm.

Comparison between the images and the plots indicates a clear correspondence to the partially visible remains. Specifically, the enclosure wall of the churchyard, the boundary wall of the homefield, a central structure within the churchyard and structures (e.g., booths) within the homefield are characterized by relatively low and high values of apparent ground conductivity and in-phase, respectively. These responses are most likely due to rocks.

Figures 9 and 10 present comparisons of in-phase data (sensor 2) from 2013 and 2015, respectively, based on using different image processing schemes. The schemes include normal histogram, equalization histogram and equalization histogram of the residual after background removal of a second-order polynomial trend. Highlighted in red are several partially exposed archaeological remains, which include booths and sections of the homefield's boundary wall. The comparisons demonstrate that the schemes based on equalization histogram provide a better correspondence to the known archaeology. In general, the equalization histogram is useful when the dynamic range of a dataset is low, thus enhancing small-contrast values.

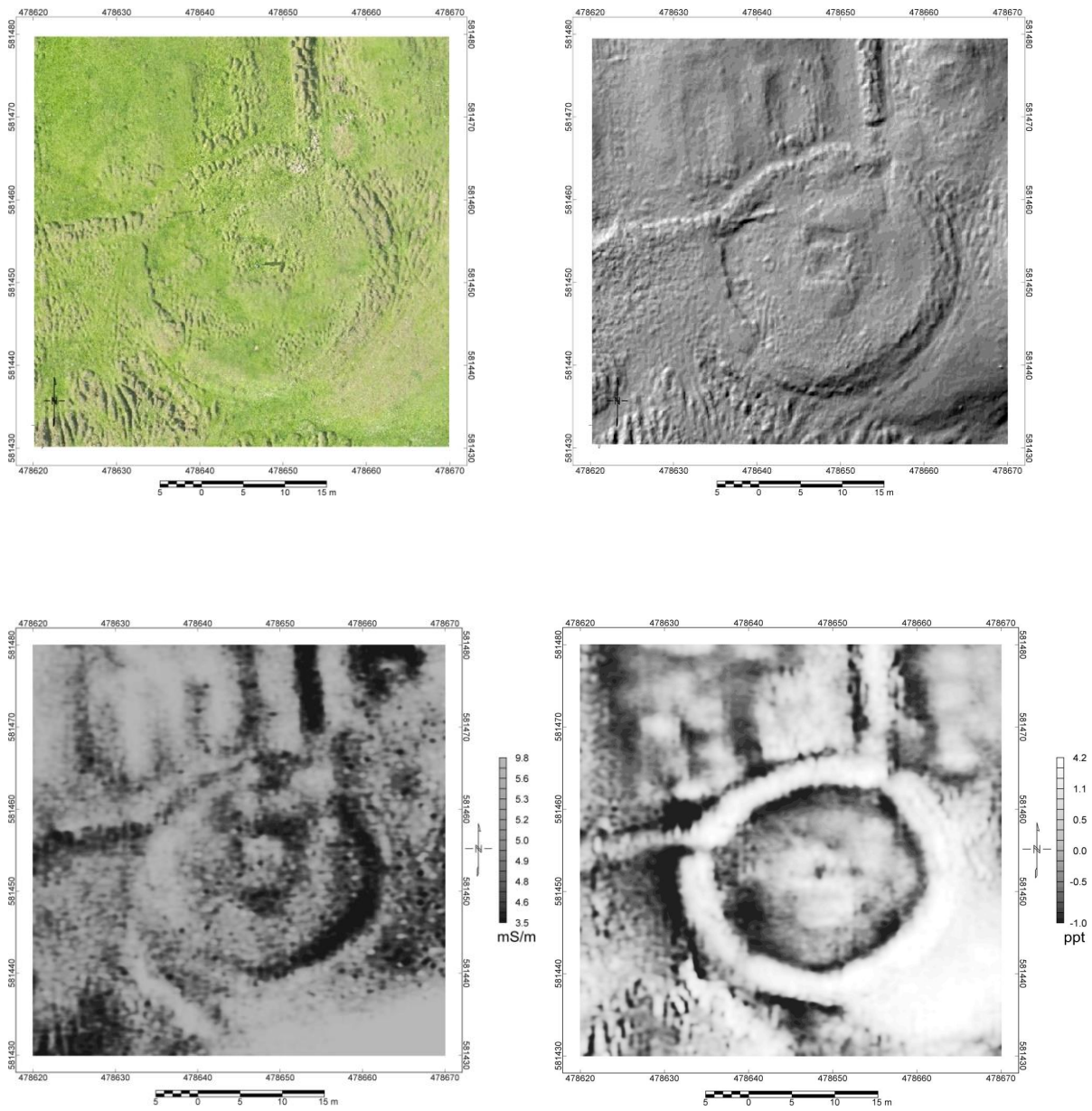


Figure 3. Results of FDEM survey conducted in 2013. Upper Left: Optical topographic image of area that was obtained by kite-based photography. Upper Right: Hill-shaded topographic image. Lower Left: Gray-shaded plot of apparent ground conductivity data (sensor 2, dipole length = 2.82 m). Lower Right: Gray-shaded plot of corresponding in-phase.

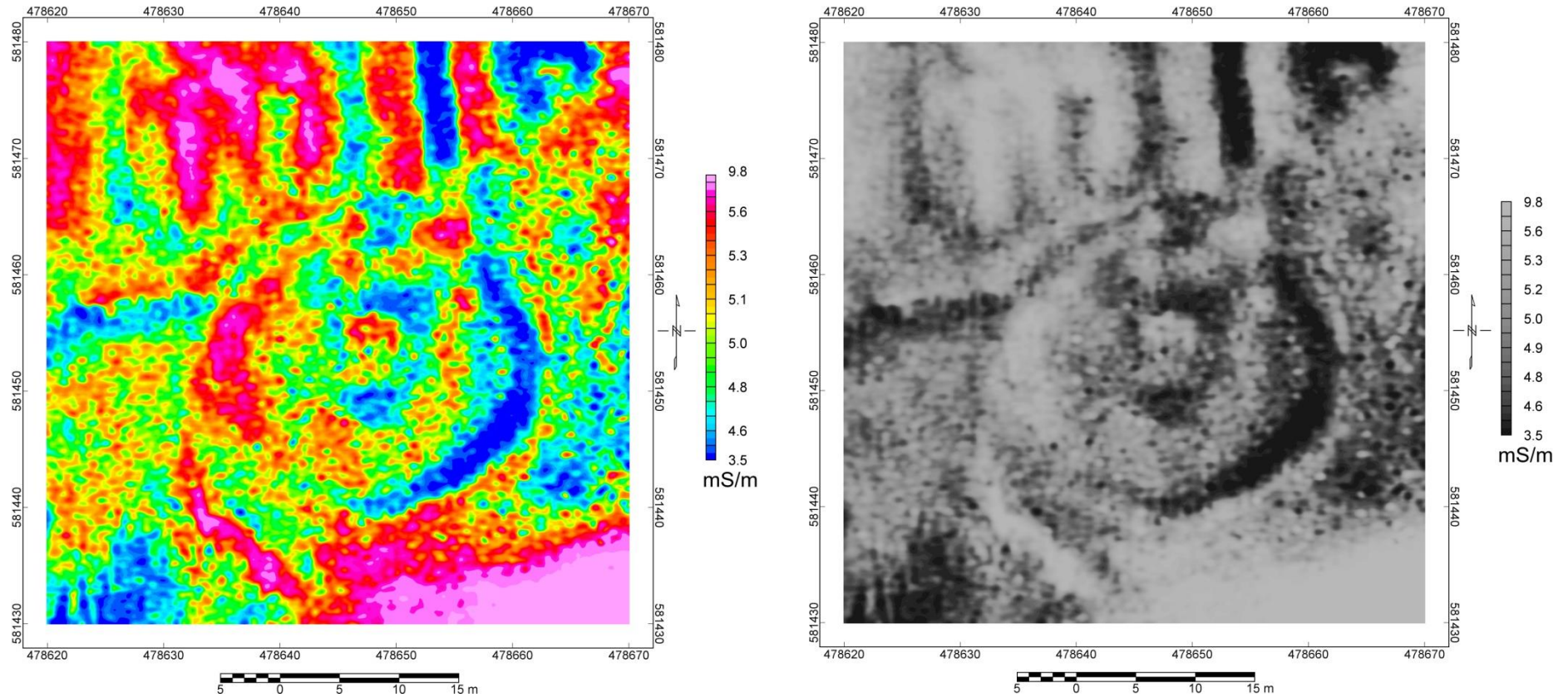


Figure 4. Left: Color-contour plot of apparent ground conductivity data (sensor 2, dipole length = 2.82 m) from survey conducted in 2013. Right: Gray-shaded plot.

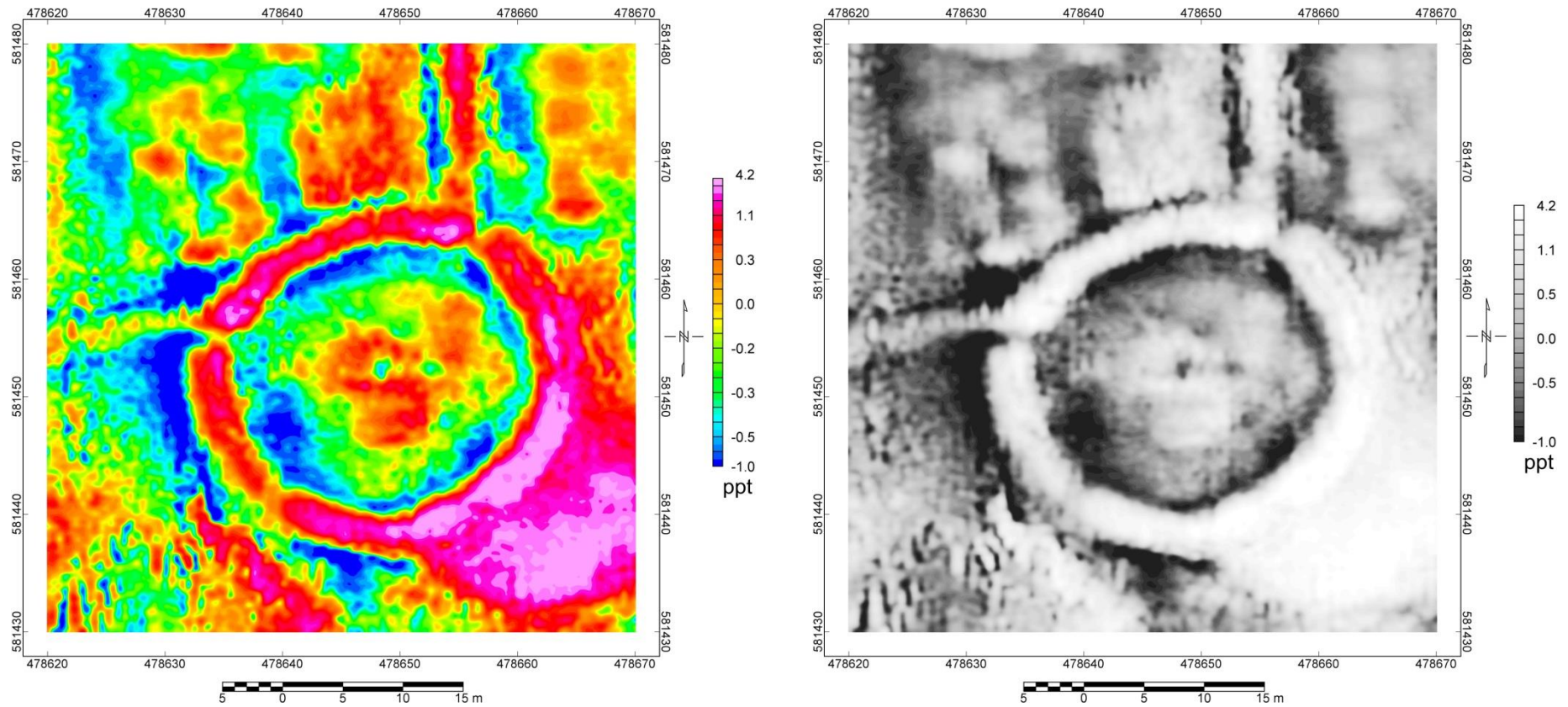


Figure 5. Left: Color-contour plot of in-phase data (sensor 2, dipole length = 2.82 m) from survey conducted in 2013. Right: Gray-shaded plot.

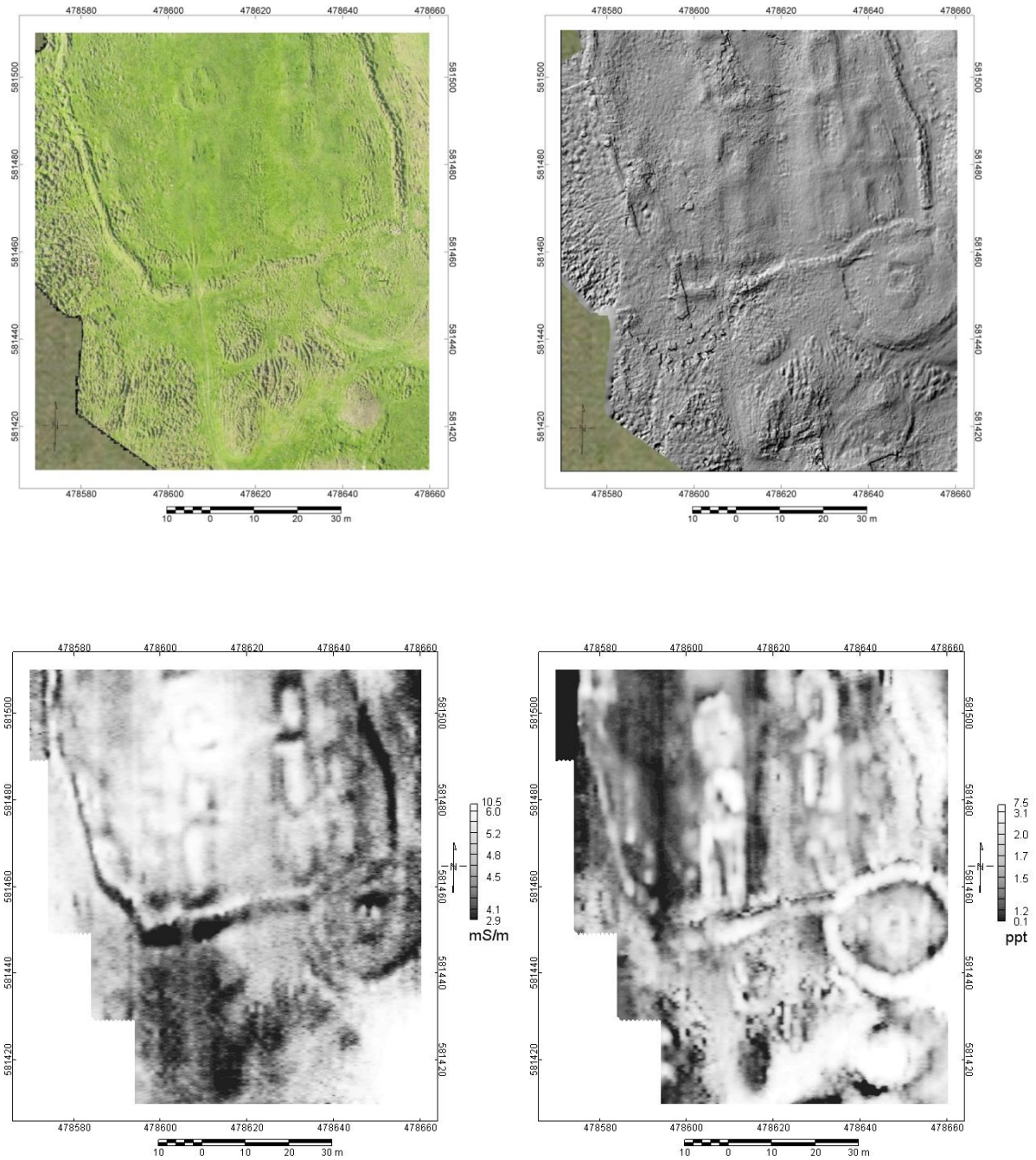


Figure 6. Results of FDEM survey conducted in 2015. Upper Left: Optical topographic image of area that was obtained by kite-based photography. Upper Right: Hill-shaded topographic image. Lower Left: Gray-shaded plot of apparent ground conductivity data (sensor 2, dipole length = 2.82 m). Lower Right: Gray-shaded plot of corresponding in-phase.

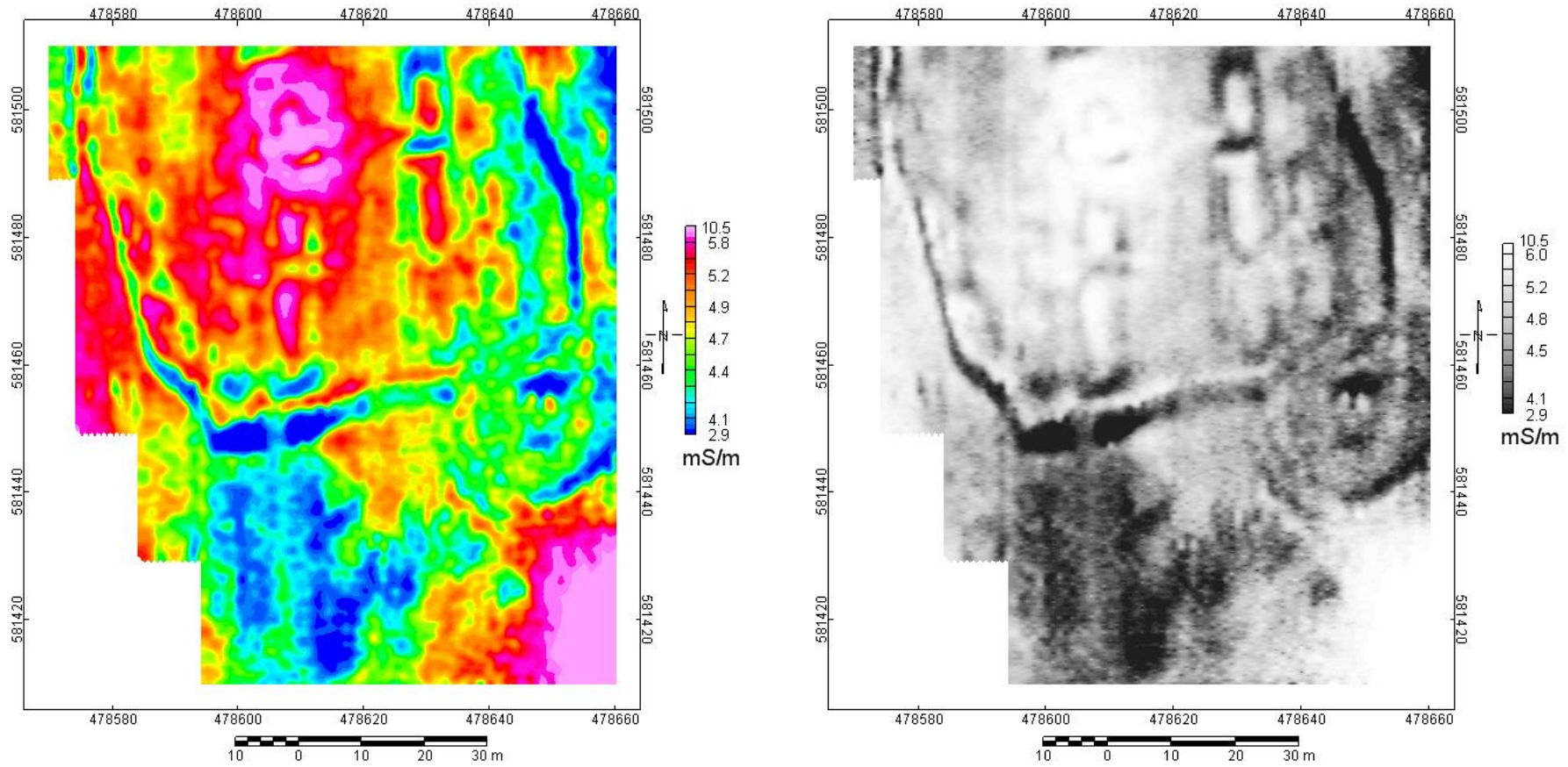


Figure 7. Left: Color-contour plot of apparent ground conductivity data (sensor 2, dipole length = 2.82 m) from survey conducted in 2015. Right: Gray-shaded plot.

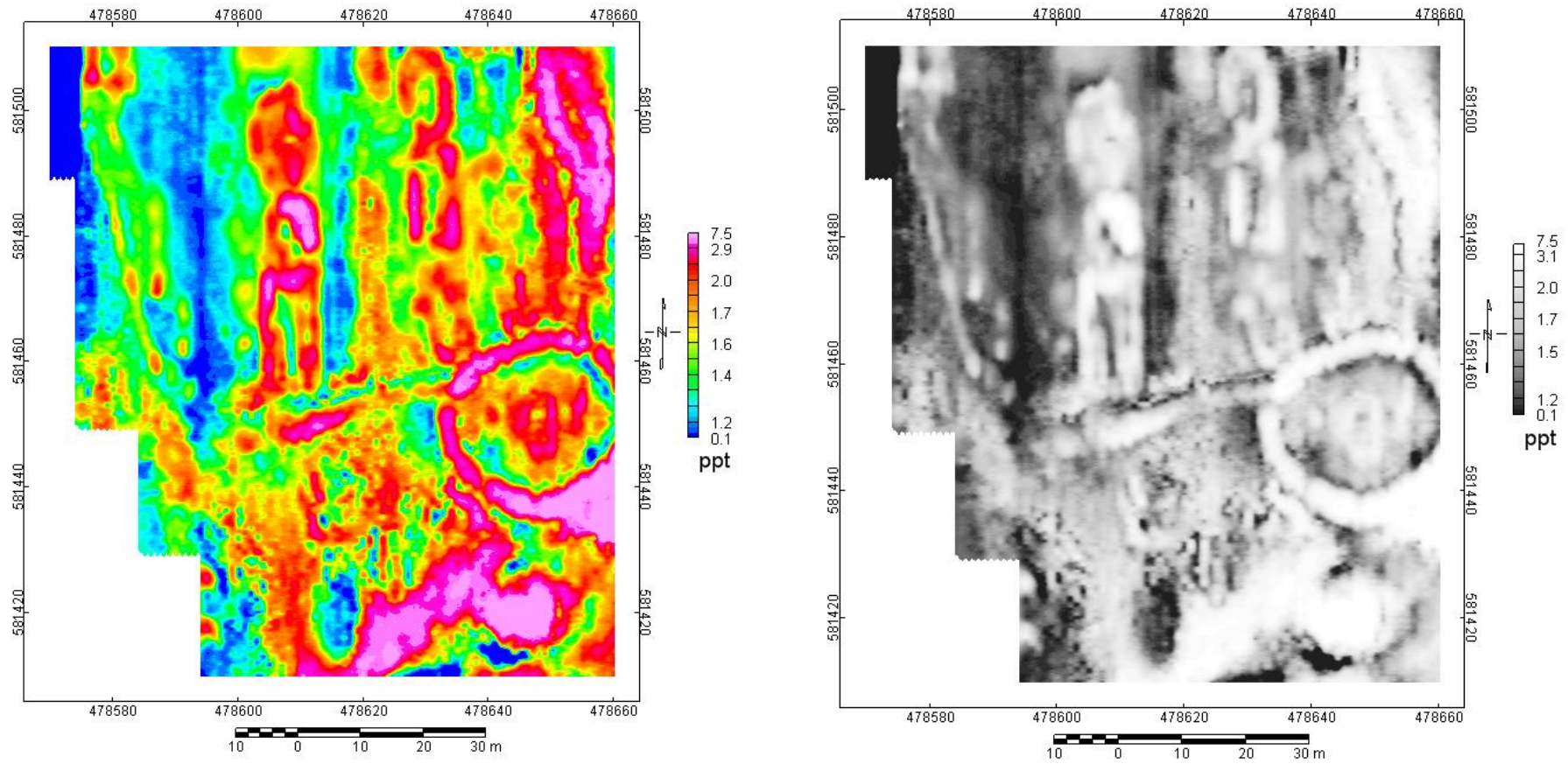


Figure 8. Left: Color-contour plot of in-phase data (sensor 2, dipole length = 2.82 m) from survey conducted in 2015. Right: Gray-shaded plot.

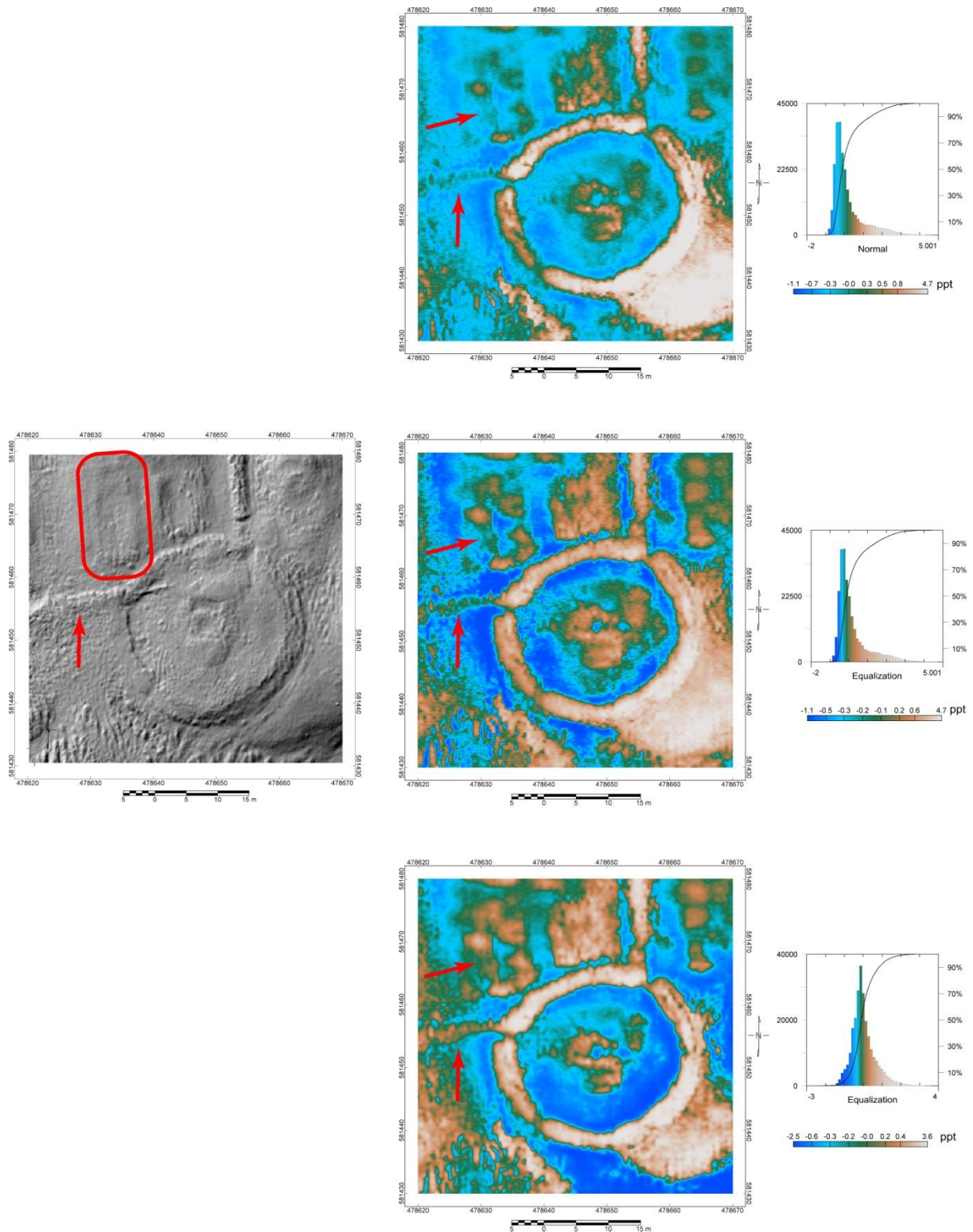


Figure 9. Comparison of in-phase data (sensor 2, dipole length = 2.82 m) from survey conducted in 2013. Middle Left: Hill-shaded topographic image. Upper Right: Data plotted based on normal histogram. Middle Right: Data plotted based on equalization histogram. Lower Right: Data plotted based on equalization histogram of the residual after background removal (second-order polynomial trend). Red rectangle and arrows highlight partially exposed archaeological remains (booth and a section of the homefield's boundary wall).

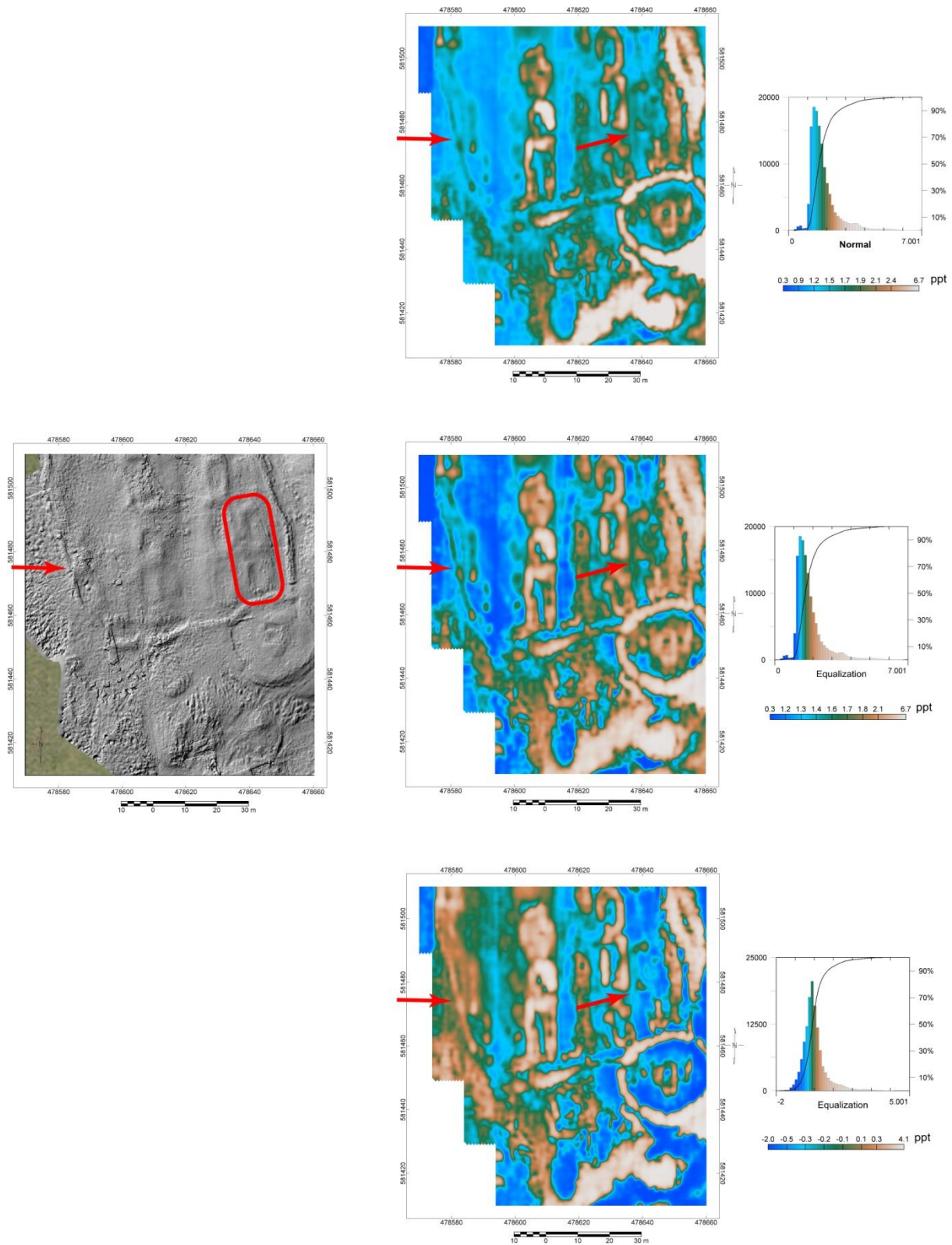


Figure 10. Comparison of in-phase data (sensor 2, dipole length = 2.82 m) from survey conducted in 2015. Middle Left: Hill-shaded topographic image. Upper Right: Data plotted based on normal histogram. Middle Right: Data plotted based on equalization histogram. Lower Right: Data plotted based on equalization histogram of the residual after background removal (second-order polynomial trend). Red rectangle and arrows highlights partially exposed archaeological remains (booths and a section of the homefield’s boundary wall).

3.3 Time-Domain Reflectometry

Time-domain reflectometry is commonly used in the soil sciences to indirectly measure the moisture content of soils by directly measuring its relative permittivity (ϵ_r). Relative permittivity is an electromagnetic property that provides a measure of how easily a material can become polarized by imposition of an electric field. It is the contrasts in relative permittivity between soil and materials comprising archaeological features that give rise to the reflections that are measured by GPR. Thus, an assessment as to the likelihood of detecting archaeological features can be made based on measuring the relative permittivity of the background soil, with specific emphasis on the detection of skeletal remains ($\epsilon_r = 5-13$; see Damiata et al., 2013).

3.3.1 Equipment and Field Procedures

Time-domain reflectometry measurements were collected at three random locations adjacent to and within the churchyard. The measurements were made using a Trase 6050X1 instrument (Soilmoisture Equipment Corp®, Santa Barbara, CA, USA) which consists of two parallel stainless steel rods that form the waveguide (Figure 11). The rods are 0.3 m in length, 6 mm in diameter and spaced 0.05 m apart. The probe was inserted vertically into the prevailing ground surface. Typically, a set of four measurements were made at a given sampling location. Prior to collecting a measurement, the probe was zeroed (short circuited) and a measurement was made in air ($\epsilon_r = 1$) to ensure proper functioning of the instrument.

3.3.2 Data Processing

The apparent relative permittivity was initially calculated using WinTrase software (v. 2.07) which employs the standard tangent-line fitting procedure to determine the times of reflection.

3.3.3 Results

The three measured values of apparent relative permittivity were: 22.7, 32.1, and 27.9, which averages to ~ 28 . Using this value and neglecting any potential dispersion yields a radar-wave velocity of ~ 0.06 m/ns, which was used to convert the GPR time slices into depth slices. This representative value also indicates that any well-preserved skeletal remains subject to simple burial conditions (e.g., burial shafts cut into a uniform soil) are potentially detectable using

GPR, neglecting complicating factors such as complex stratigraphy due to the presence of gravel or non-uniform fill.



Figure 11. Photograph of the Trase 6050X1 TDR instrumentation.

3.4 Ground-Penetrating Radar

In 2013, a GPR survey was conducted over a 14 x 15 m grid, which was located over a part of the cemetery of the churchyard (see Figure 1). The primary objective was to evaluate whether unmarked burials could be detected with GPR within its confines. The use of GPR to detect unmarked burials and clandestine graves has been reported widely in the archaeological, forensic sciences, and geophysical literature (e.g., Bevan 1991; Buck 2003; Conyers 2006; Schultz 2007; Ruffell et al. 2009; Fiedler et al. 2009; Doolittle & Bellantoni 2010; Goodman et al. 2007), and has been successfully applied previously at the nearby Stóra Seyla farm (Damiata et al., 2013).

As to whether a burial is detectable by GPR depends on various factors. In particular, a measureable contrast in the geophysical (electromagnetic) property of relative permittivity must exist between the combined elements of a burial and the surrounding naturally compacted soil. The elements of a burial that determine its relative permittivity include: (1)

soil moisture content, (2) ground disturbance caused by digging and filling the grave shaft which homogenizes the backfill soil and introduces small air voids into it, (2) skeletal remains, (3) grave goods of sufficient size, if present, and (4) container such as a shroud, vault, coffin or casket, if any. In some instances, a measureable contrast may not exist even though a burial is present. For these cases, the contrast between burial elements and the surrounding undisturbed soil was either insufficient initially or had diminished with time because of, for example, the disintegration of skeletal remains by natural decomposition or through interaction with the local environment. Based on previous efforts at the nearby Stóra Seyla farm, the ground conditions seem particularly suited for the detection of skeletal remains by using GPR. Summarized below are the field procedures, data analysis and results of the GPR survey that was conducted over a part of the cemetery at Hegranesþing.

3.4.1 Equipment and Field Procedures

The GPR survey was performed using a Malå X3M system that was equipped with a 500 MHz antenna (Figure 12). Data were collected at a vertical scan interval of approximately 0.02 m along parallel contiguous transects that were separated by 0.2 m. The data collection was guided by stretching a fiberglass measuring tape between the endpoints of 1-m spaced transects. However, the actual location was determined by inserting fiducial markers into the data stream at 1-m intervals (as marked on the measuring tapes) by the operator, and assuming linear interpolation between markers. The survey was conducted in a uni-directional manner (i.e., from south to north). In total, 71 radar profiles were collected and 1,065 linear meters were traversed for the survey.

3.4.2 Data Processing

The data were processed using GPR-Slice software (see www.gpr-survey.com; Goodman *et al.* 1995; Goodman *et al.* 2007; Goodman *et al.* 2008). The raw vertical scan data were gained, resampled and filtered (background removal and boxcar) to produce processed 2-D radargrams. On these radargrams, the presence of strong reflectors is indicated by a black-and-white banding pattern. Note that the raw data were collected in terms of the two-way travel time of reflected energy. To convert to a depth scale, a radar wave velocity of 0.057 m/ns was assumed based on a relative permittivity value of 27.6. The processed radargrams were next combined to produce a pseudo three-dimensional data set. A total of sixty

horizontal depth-slice images of approximately 0.05 m with 50% overlap were initially generated to provide detailed spatial information on the location and depth of reflectors (i.e.,



Figure 12. Photograph of the Mala X3 equipped with a 500 MHz antenna.

horizontal plan of strong reflectors at a specific interval of depth that combines data from all radargrams). Overlay depth images were then produced by combining (binning) depth-slice images into 0.25-m-thick intervals, as presented in Figure 13. Annotated radargrams are presented in Appendix D.

3.4.3 Results

The overlay depth-slice images revealed two interesting geometric elements. The first is an arcuate set of strong reflections in the eastern part at depths of 50 to 70 cm. Although speculation, these reflections would be consistent with an earlier circular enclosure wall. The second is a rectilinear set of strong reflections in the western part at depths of 100 to 125 cm. These reflections occur in the center of the churchyard and would be consistent with the foundation of a church.

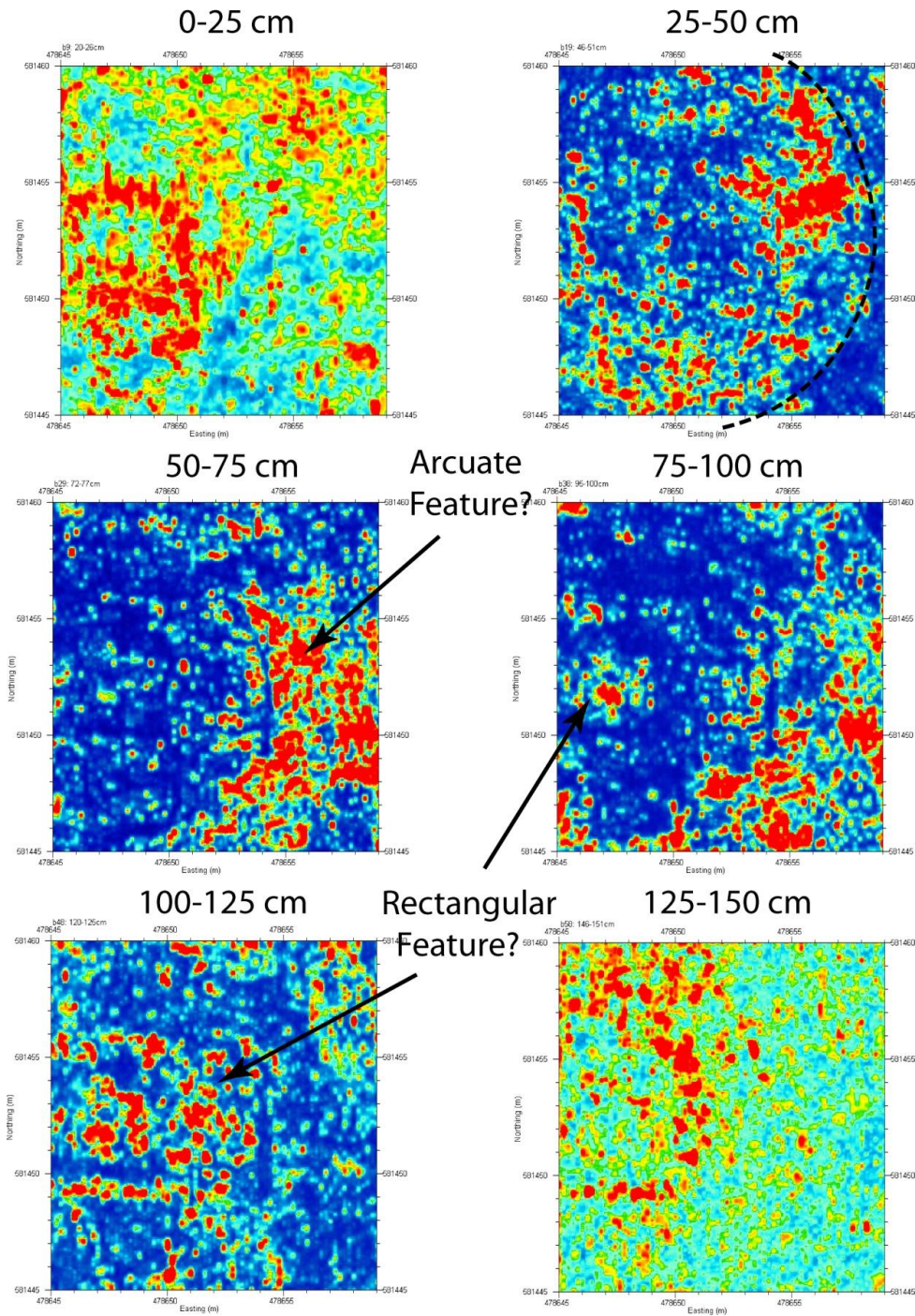


Figure 13. Overlay depth-slice images from GPR survey conducted in 2013 in the eastern inner part of cemetery at Hegranesþing (see Figure 1 for location). Strong reflections are denoted in red.

Table 1. Interpreted below-ground burials associated with GPR reflections; see Appendix D for annotated radargrams.

Grave ID	Starting/Ending Profile	Length (m)	Northing ⁽¹⁾	Easting ⁽¹⁾	Approximate Depth to Top (m)	Comments
1	5257 – 5265	1.6	455.7 – 455.8	647.2 – 648.8	0.55 – 0.65	
2	5259 – 7660	1.0	458.6 – 458.6	647.6 – 648.6	0.80 – 0.90	
3	5270 – 5280	2.0	458.1 – 458.3	649.8 – 651.8	0.50 – 0.75	extends to East?
4	5270 – 5274	0.8	459.3 – 459.2	649.8 – 650.6	0.45 – 0.60	
5	5276 – 5283	1.4	457.7 – 457.7	651.0 – 652.4	0.40 – 0.55	
6	5278 – 5285	1.4	458.7 – 458.7	651.4 – 652.8	0.40 – 0.55	conflated with 7?; extends to East?
7	5278 – 5285	1.4	459.0 – 459.1	651.4 – 652.8	0.40 – 0.55	conflated with 6?; extends to East?
8	5279 – 5285	1.2	457.1 – 457.1	651.6 – 652.8	0.85 – 0.95	

¹ Add 581,000 to Northing; add 478,000 to Easting

Lastly, eight burials have been tentatively identified based on detailed inspections of individual radargrams (see Table 1 and Figure 14). Skeletal remains are likely present given that several had already been excavated from the cemetery (Zoëga, 2009). As previously noted, the TDR measurements indicated favorable conditions for their detection by GPR. It is suspected that more burials may exist; however, detection by GPR has been hampered by a combination of factors including: 1) a hummocky ground surface which resulted in inaccuracies in true location, thus making it difficult to trace coherent reflections from the same source on contiguous radargrams, 2) surveying on thick grass probably attenuated the radar's energy due to non-ideal coupling with the antenna, and (3) complex stratigraphy involving gravel layers and reworked fill deposits has most likely obscured reflections emanating from the skeletal remains. Deturfing the ground surface would improve the quality of data, at least with respect to the first two issues, for any future-planned GPR surveying.

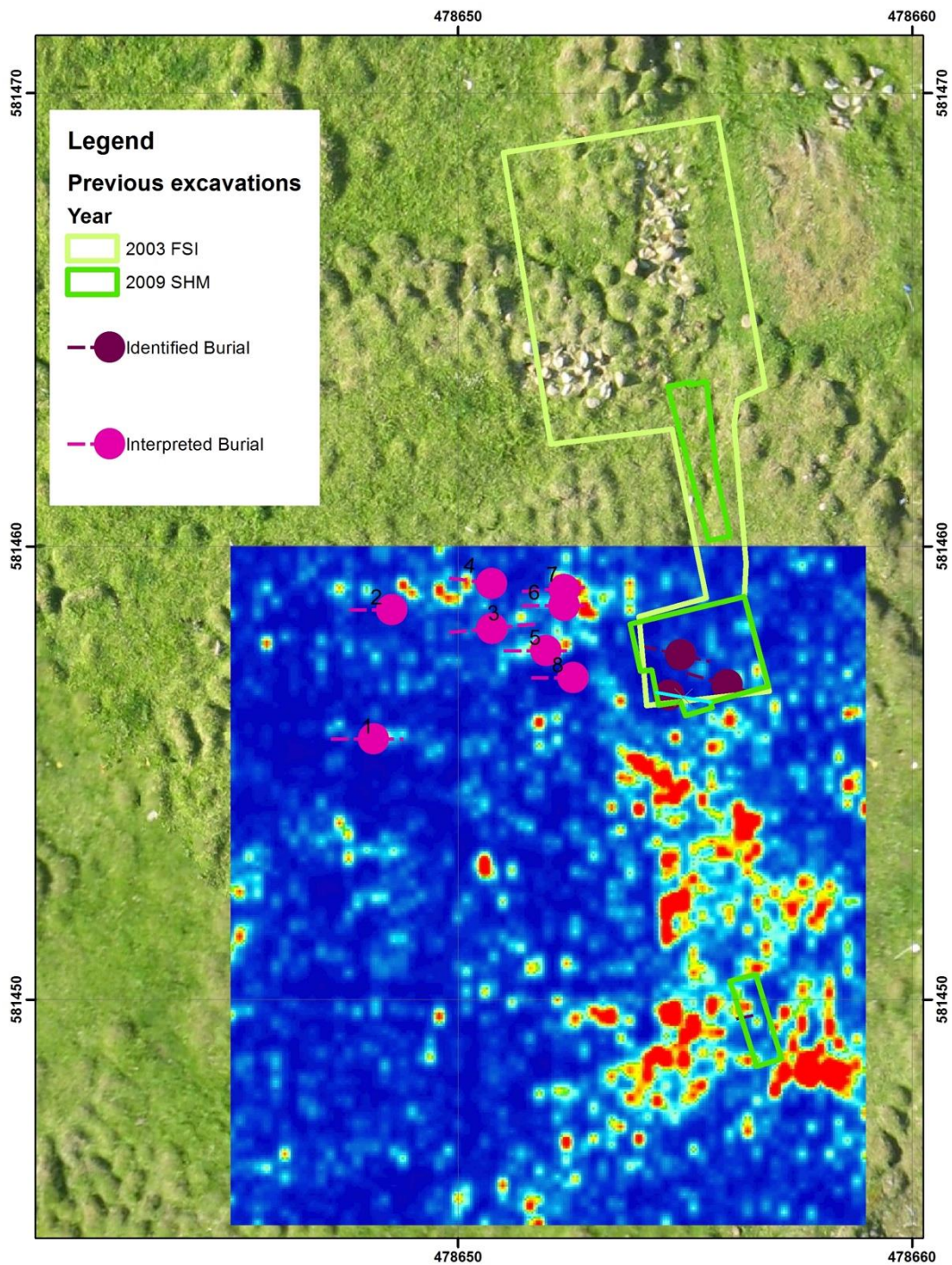


Figure 14. Interpreted below-ground burials from Table 1 superimposed on GPR Slice 27 (102-110 cm bgs – Appendix E), superimposed on kite air photo. Also shown are 2003 and 2009 excavations and burials identified in those excavations (Zoëga, 2009).

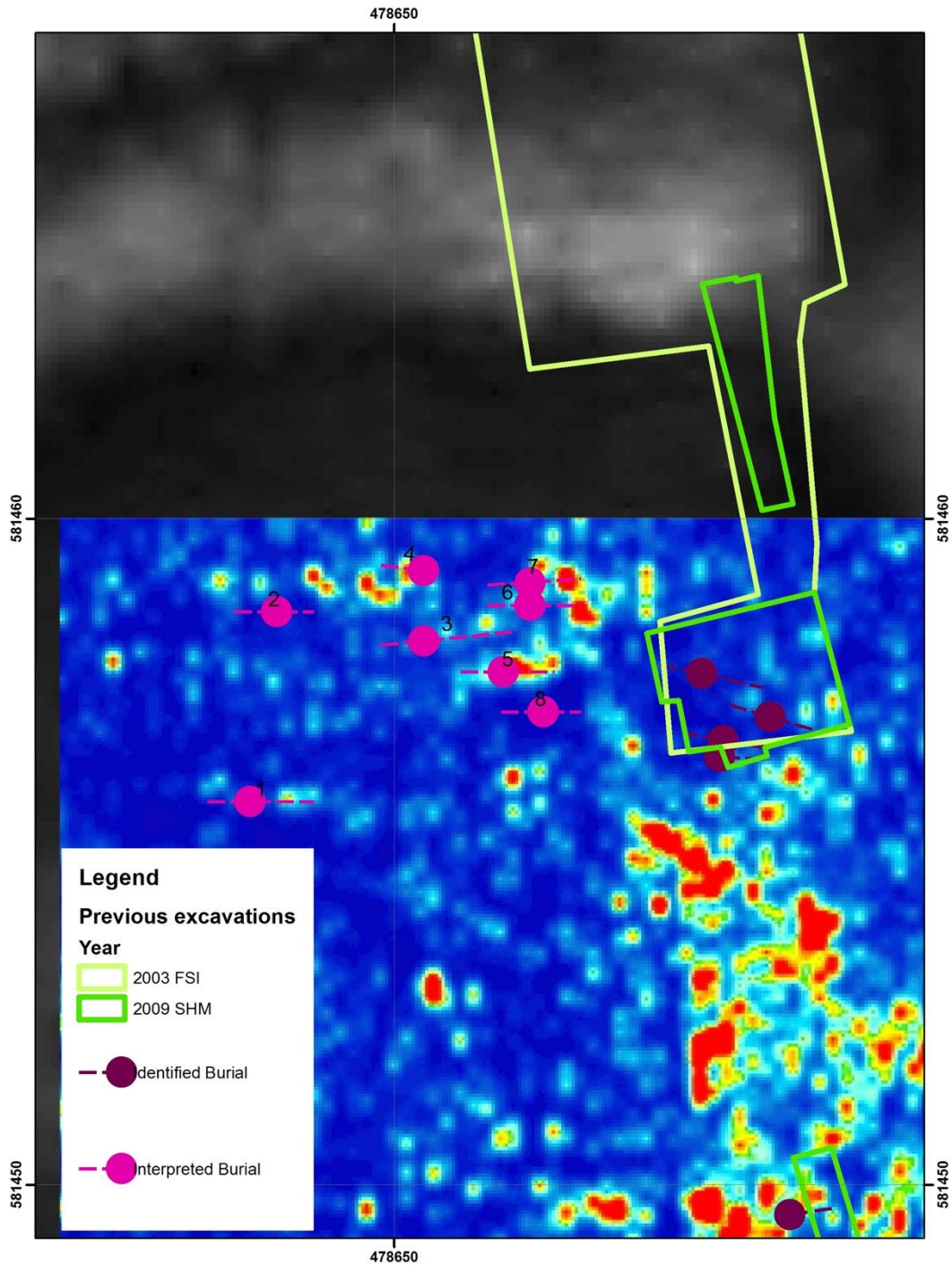


Figure 15. Close up of interpreted below-ground burials from Table 1 superimposed on GPR Slice 27 (102-110 cm bgs – Appendix E), superimposed on FDEM in-phase sensor 2 (Figure 8). Also shown are 2003 and 2009 excavations and burials identified in those excavations (Zoëga, 2009).

4.0 SUMMARY AND CONCLUSIONS

Geophysical surveys were conducted at Hegranesþing in 2013 and 2015. The work included FDEM surveys of the churchyard and the surrounding area, as well as a GPR survey that was limited to the eastern half of the churchyard. The site provided a convenient means to evaluate the effectiveness of the methods given the substantial amount of archaeological remains that are partially exposed. Eight additional graves were identified, and their orientation fit nicely with the others previously identified (Zoëga 2009).

The FDEM data from sensor 2 provided the best correspondence to the visible remains, which included the enclosure wall of the churchyard, the boundary wall of the homefield, a central structure within the churchyard and structures (e.g., booths) within the homefield. These features are characterized by relatively low and high values of apparent ground conductivity and in-phase, respectively. These responses are most likely due to rocks. Presenting the data based on equalization histogram appears to be particularly suited to enhance subtle contrasts.

The FDEM sensor 2 results around E 478610 N 581500 (e.g., Figure 7) are high, but not well defined, and suggest the possible presence of a long-term domestic occupation which may potentially be Litli-Garður or an earlier occupation at that same location. This broad anomaly is qualitatively different from the well-defined smaller booth anomalies seen in other parts of the site. This is potentially a farmstead but it will require archaeological data to confirm its nature

The results of the GPR survey included the delineation of arcuate and rectilinear features. The latter is probably a rock foundation of the church. In addition, eight burials have been tentatively identified. Removal of the turf would and leveling of the ground surface would improve the quality of data for any future intended surveying by GPR.

5.0 REFERENCES

- Arnalds, Ó. 2004. "Volcanic soils of Iceland," *Catena* 56: 3-20.
- Arnalds, Ó. 2008. "Soils of Iceland," *Jokull* 58: 409-421.
- Arnalds, Ó., C. T. Hallmark, and L. P. Wilding. 1995. "Andisols from 4 Different Regions of Iceland," *Soil Science Society of America Journal* 59: 161-169.
- Bevan, B. W. 1991. "The search for graves," *Geophysics* 56: 1310-1319.
- Conyers, L. B. 2005. *Ground-Penetrating Radar for Archaeology*. Lanham, MD: Altamira Press.
- Conyers, L. B. 2006. "Ground-Penetrating Radar Techniques to Discover and Map Historic Graves," *Historical Archaeology* 40: 64-73.
- Damiata, B. N., J. M. Steinberg, D. J. Bolender, and G. Zoëga. 2013. "Imaging skeletal remains with ground-penetrating radar: comparative results over two graves from Viking Age and Medieval churchyards on the Stóra-Seyla farm, northern Iceland," *Journal of Archaeological Science* 40: 268-278.
- Doolittle, J. A., and N. F. Bellantoni. 2010. "The search for graves with ground-penetrating radar in Connecticut," *Journal of Archaeological Science* 37: 941-949.
- Friðriksson, A., C. Batey, H. Gestsdóttir, Garðar Guðmundsson, M. Á. Sigurgeirsson, H. M. Roberts, and J. Wollett. 2004. Þinghald að Fornufornleifarannsóknir 2003. Reykjavík: Fornleifastofnun Íslands (FSÍ).
- Gaffney, C., and J. Gater. 2003. *Revealing the buried past : geophysics for archaeologists*. Stroud: Tempus.
- Goodman, D., Y. Nishimura, and J. D. Rogers. 1995. "GPR time slices in archaeological prospection," *Archaeological Prospection* 2: 85-89.
- Goodman, D., S. Piro, Y. Nishimura, K. Schneider, H. Hongo, N. Higashi, J. Steinberg, and B. Damiata. 2008. "GPR Archaeometry," In *Ground Penetrating Radar Theory and Applications*, edited by H. Jol. New York: Elsevier, 479-508.
- Goodman, D., J. Steinberg, B. Damiata, Y. Nishimura, S. Piro, and K. Schneider. 2007. "GPR Imaging of Archaeological Sites," In *Reconstructing Human-Landscape Interactions, Dig 2005 Conference, Developing International Geoarchaeology*, edited by L. Wilson, P. Dickinson and J. Jeandron. Cambridge: Cambridge Scholars Publishing, 202-217.
- Grab, S. 2005. "Aspects of the geomorphology, genesis and environmental significance of earth hummocks (thufur, pounus): miniature cryogenic mounds," *Progress in Physical Geography* 29: 139-155.
- Jones, G. 2008. "Geophysical Mapping of Historic Cemeteries," *Technical Briefs in Historical Archaeology* 3: 25-38.
- King, J. A., R. J. Hurry, and B. W. Bevan. 1993. "Reliability of geophysical surveys at historic-period cemeteries: an example from the Plains cemetery, Mechanicsville, Maryland," *Historical Archaeology* 27: 4-16.
- Linford, N. 2006. "The application of geophysical methods to archaeological prospection," *Reports on Progress in Physics* 69: 2205-2257.
- Schultz, J. J. 2008. "Sequential Monitoring of Burials Containing Small Pig Cadavers Using Ground Penetrating Radar*," *Journal of Forensic Sciences* 53: 279-287.
- Schultz, J. J., and M. M. Martin. 2011. "Controlled GPR grave research: Comparison of reflection profiles between 500 and 250 MHz antennae," *Forensic Science International* 209: 64-69.
- Zoëga, G. 2009. Skagfirska kirkjurannsóknin framvinduskýrsla 2009. Sauðárkrókur: Byggðasafn Skagfirðinga.

APPENDIX A – BASIC PRINCIPLES OF FREQUENCY-DOMAIN ELECTROMAGNETICS

The frequency-domain electromagnetic (FDEM) method is an active non-destructive geophysical method that is used to obtain shallow subsurface information. In the EM method, a time-varying magnetic field is generated by driving an alternating current through either a loop of wire or a straight wire that is grounded at both ends. Induced or eddy currents with flow within any conductive solid or fluid material that is present beneath the area of investigation. The eddy currents, in turn, generate their own magnetic fields such that at any point in space, the total magnetic field is the superposition of the primary field due to the source current and secondary fields due to the eddy currents, as schematically illustrated in Figure B1. By discriminating between primary and secondary fields, variations in the EM properties of the ground can be discerned.

EM instruments measure both out-of-phase (quadrature) and in-phase components of the induced magnetic fields. The former is a measure of the bulk apparent ground conductivity; the latter is related to magnetic susceptibility and is particularly sensitive to the presence of metallic objects. Bulk apparent ground conductivity reflects true conductivity when the subsurface is homogeneous and isotropic, which is rarely the case in practice. For heterogeneous conditions, it represents an integrated effect of the all the conductivity within the volume of ground being sensed. It does not, however, represent an average conductivity and in fact can be lower or higher than the lowest or highest subsurface conductivities, respectively. A lateral variation in the components is indicative of lateral changes in properties. The conductivity is particularly sensitive to fluid content and dissolved salts or ions. Accordingly, wet sands, clays and materials with high ion content generally have high bulk apparent ground conductivity; dry sands and crystalline rocks have low bulk apparent ground conductivity.

Ideally, EM surveys are conducted in archaeological investigations to find conductive targets in resistive environments such as middens and rammed-earthed walls. Although more subtle and difficult to detect, resistive targets such as buried stone walls and foundations can also be detected through EM surveying.

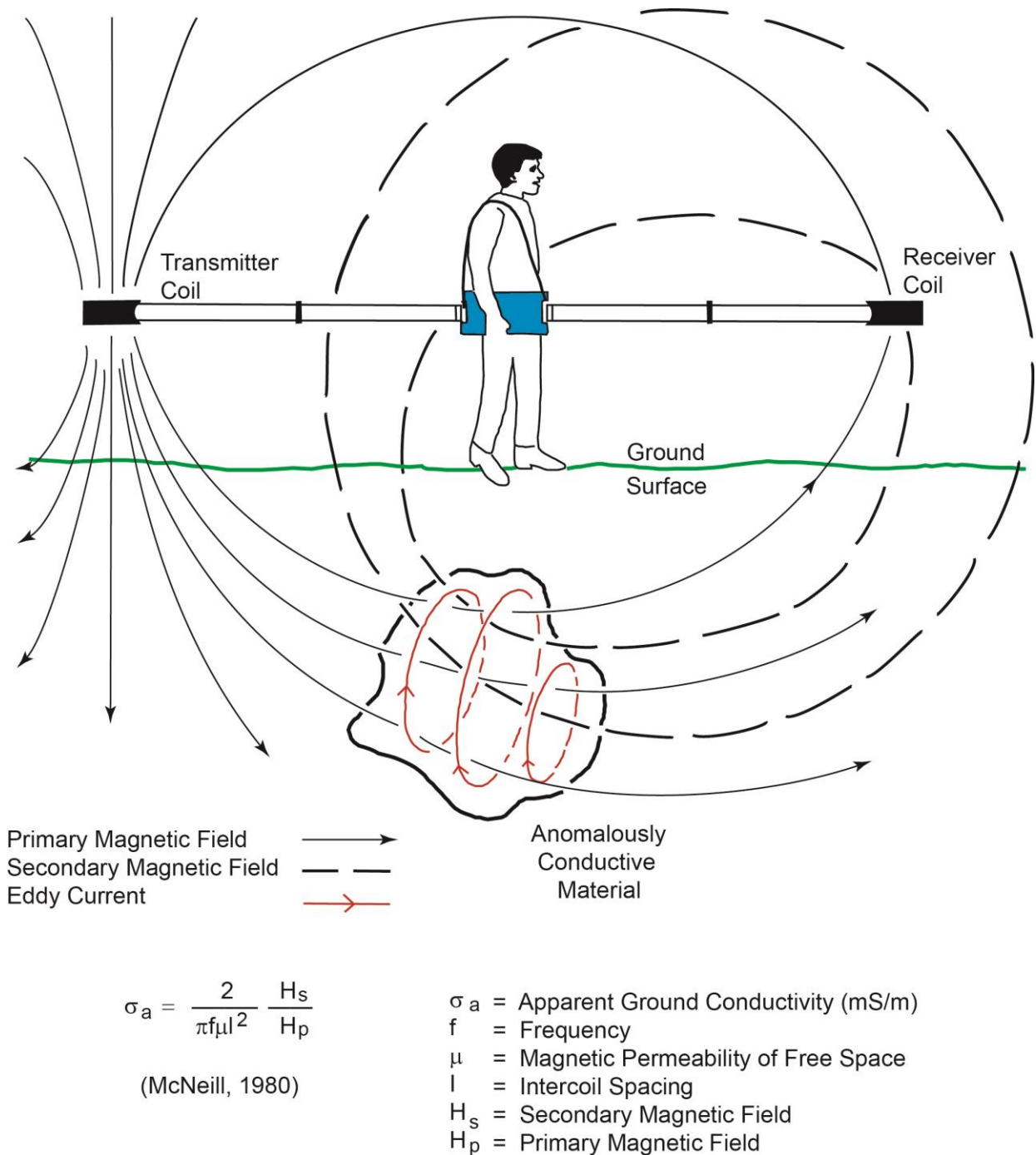


Figure A1. Schematic diagram illustrating the principles of FDEM.

APPENDIX B – BASIC PRINCIPLES OF GROUND-PENETRATING RADAR

GPR is an active non-destructive geophysical method that is used to image the shallow subsurface. In GPR, electromagnetic (EM) energy is pulsed through a transmitter antenna that is towed along the ground surface. As the energy travels through the ground and encounters distinct changes in electrical properties—specifically, the relative permittivity (E_R) which is a measure of a material’s ability to store electrical energy—a portion is reflected back to the ground surface. It is the two-way travel time of the reflected energy that is recorded by a receiver antenna in the form of a single scan at the given location as schematically illustrated in Figure B1. A two-dimensional radargram is produced by combining all of the scans along a transect. The data from many radargrams can be further combined and horizontally sliced at specified time intervals to provide pseudo-three dimensional plan images that oftentimes are easier to interpret (see accompanying figures).

Of all the available geophysical methods, GPR provides the highest possible resolution for imaging the shallow subsurface. The ability to resolved buried features, however, depends partly on the center frequency of the transmitter antenna. Relatively higher frequencies (e.g., 800 MHz) have greater resolving capabilities but at the expense of less penetrating power as compared to lower frequencies (e.g., 500 MHz). The method works best in electrically resistive conditions such as dry sandy soils. In general, electrically conductive environments can severely attenuate the EM energy. The presence of water with high dissolved solids as well as water-retaining materials such as clay and silt, even in minor amounts, can severely limit the depth of penetration.

The use of GPR should be considered whenever the target of interest provides a distinct contrast in relative permittivity (air: $E_R = 1$, water: $E_R = 81$, dry soil: $E_R = 4-6$, wet soil: $E_R = 10-30$; rock/bedrock: $E_R = 5-8$) as compared to the surroundings and is sufficient in size to be detected. Typical targets include: buried stone walls and foundations, graves, site specific stratigraphy and soil thickness/depth to bedrock.

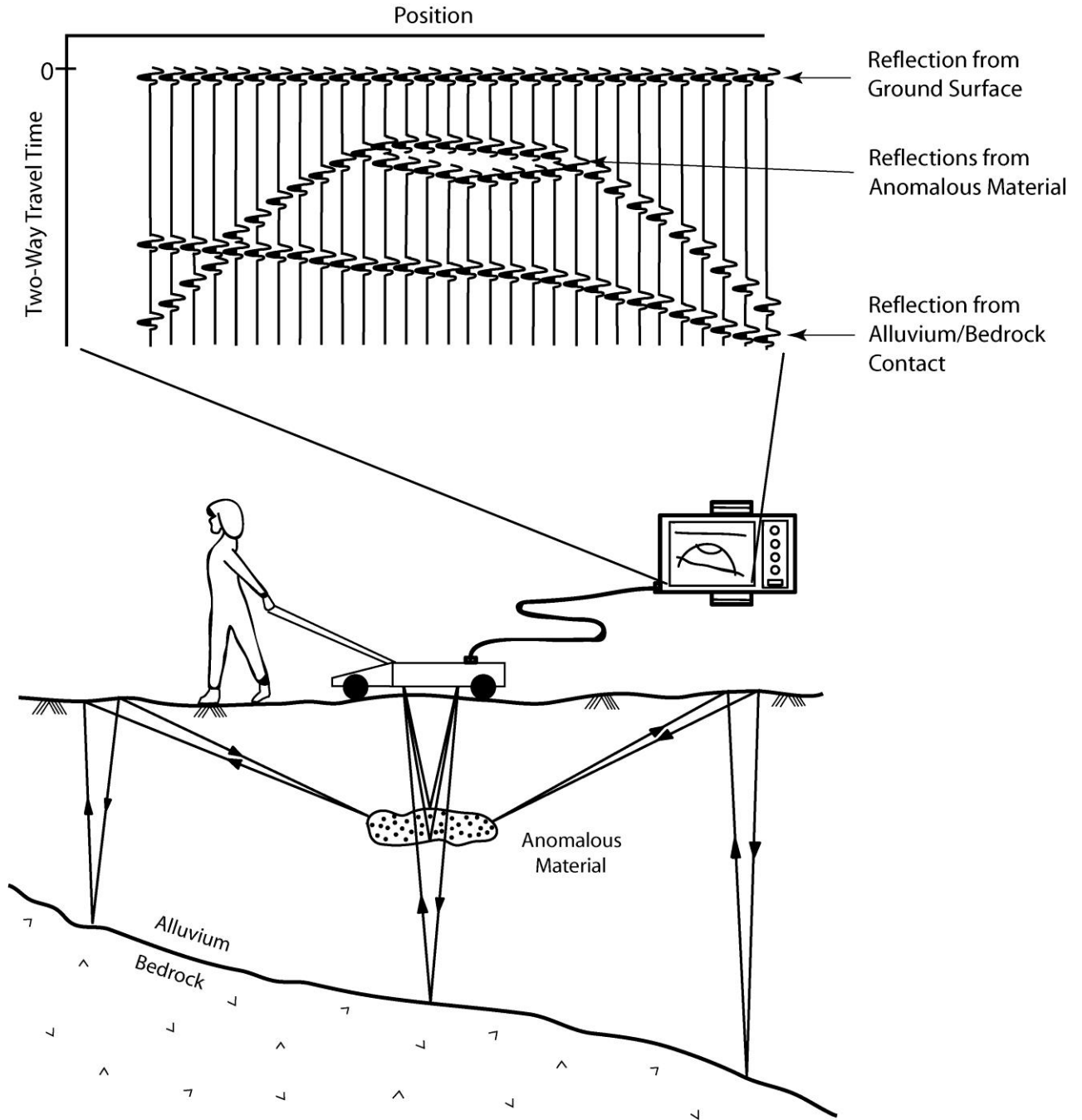


Figure B1. Schematic diagram illustrating the principles of GPR.

APPENDIX C – PLOT OF FDEM DATA

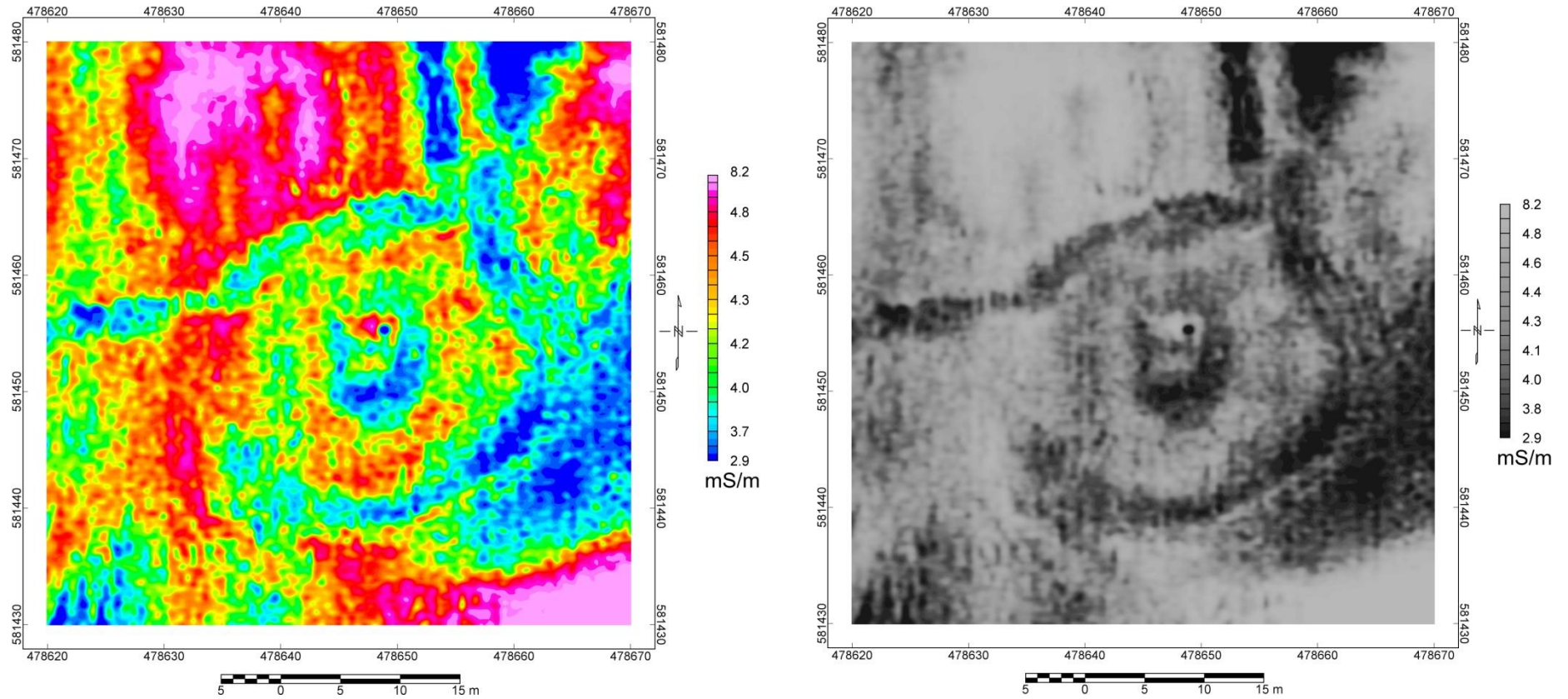


Figure C1. Left: Color-contour plot of apparent ground conductivity data (sensor 1, dipole length = 1.48 m) from survey conducted in 2013. Right: Gray-shaded plot.

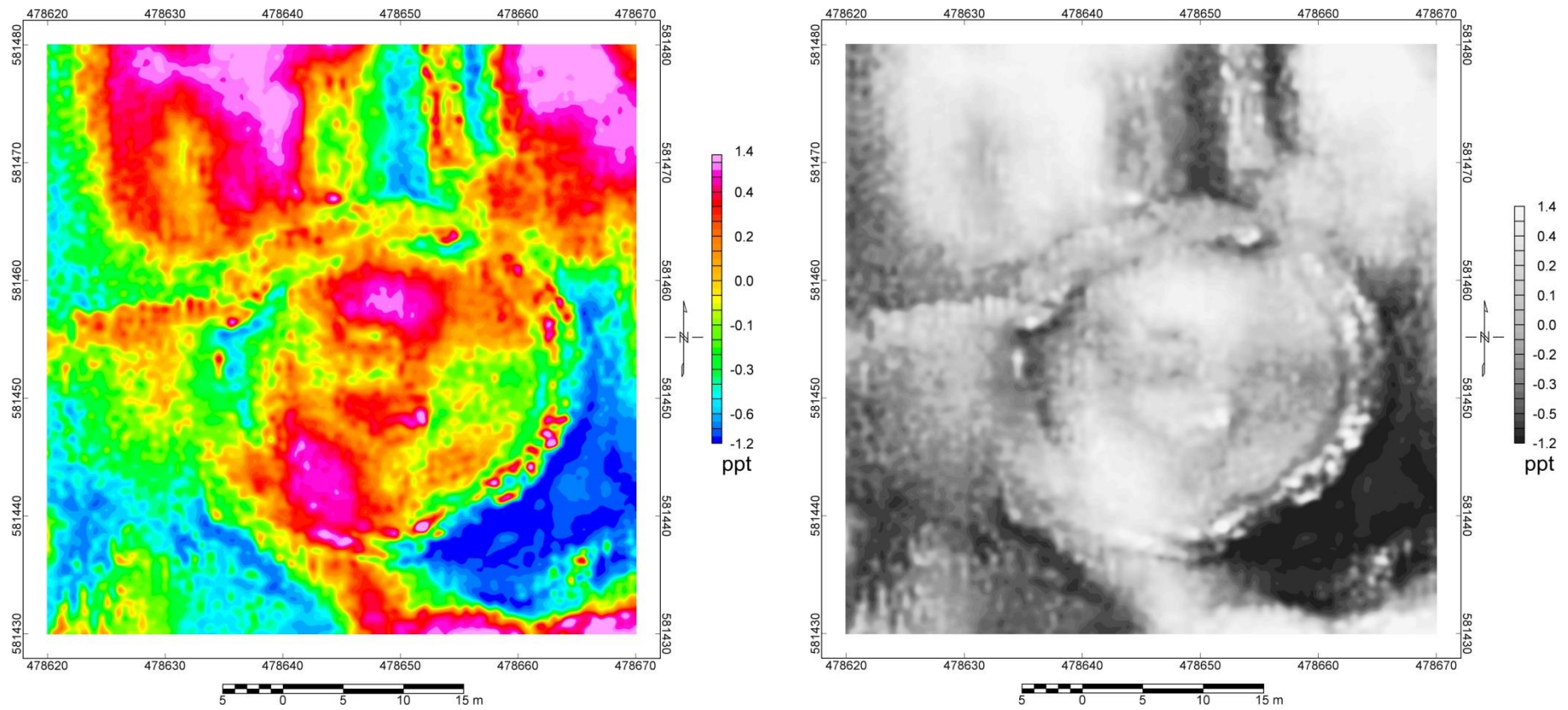


Figure C2. Color-contour plot of in-phase data (sensor 1, dipole length = 1.48 m) from survey conducted in 2013. Right: Gray-shaded plot.

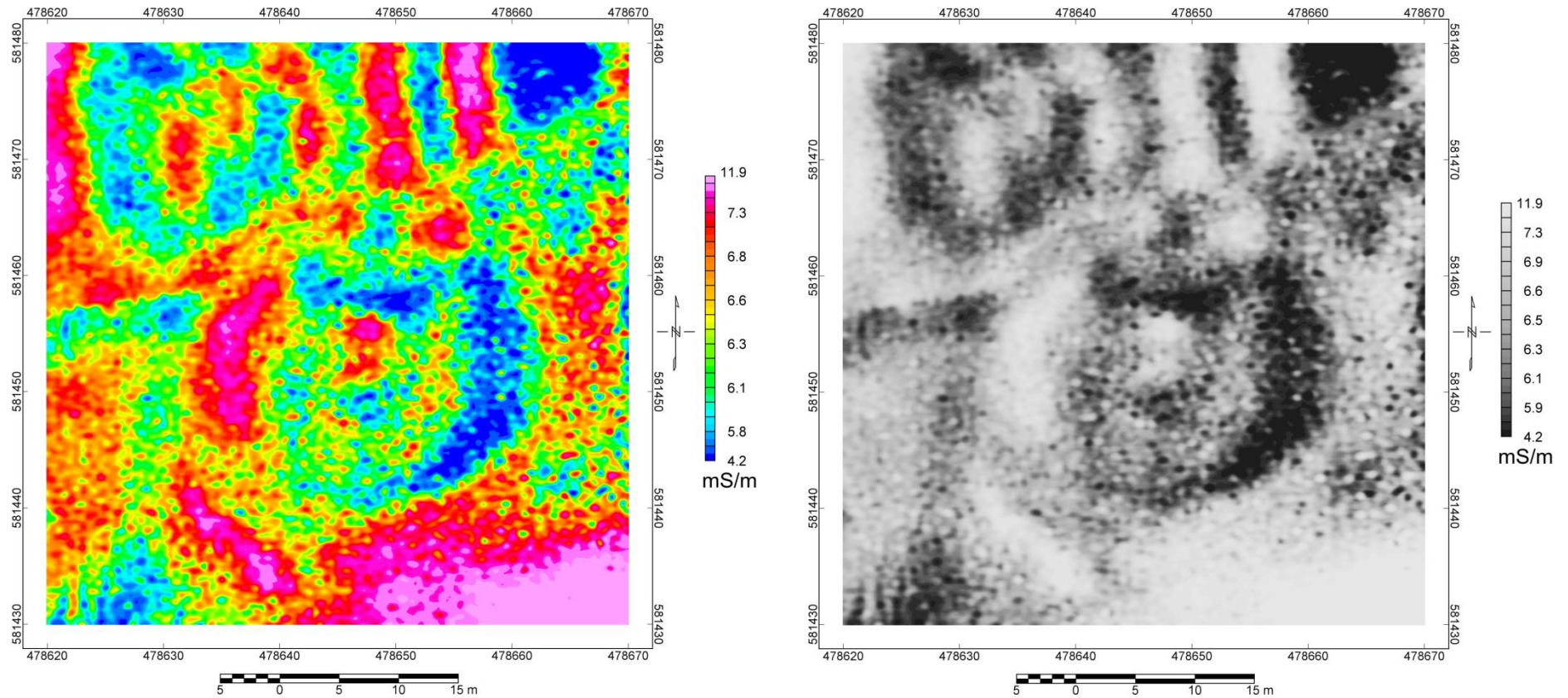


Figure C3. Left: Color-contour plot of apparent ground conductivity data (sensor 3, dipole length = 4.49 m) from survey conducted in 2013. Right: Gray-shaded plot.

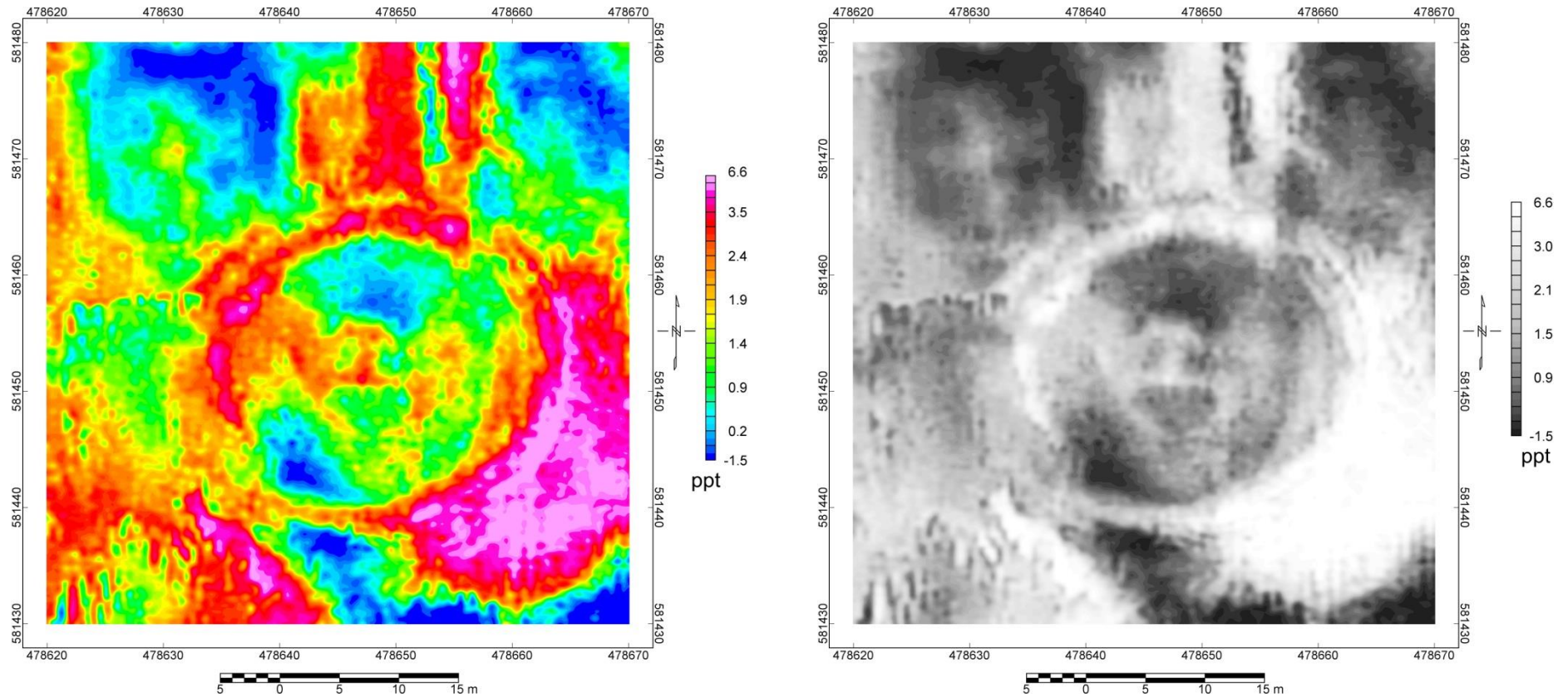


Figure C4. Color-contour plot of in-phase data (sensor 3, dipole length = 4.49 m) from survey conducted in 2013. Right: Gray-shaded plot.

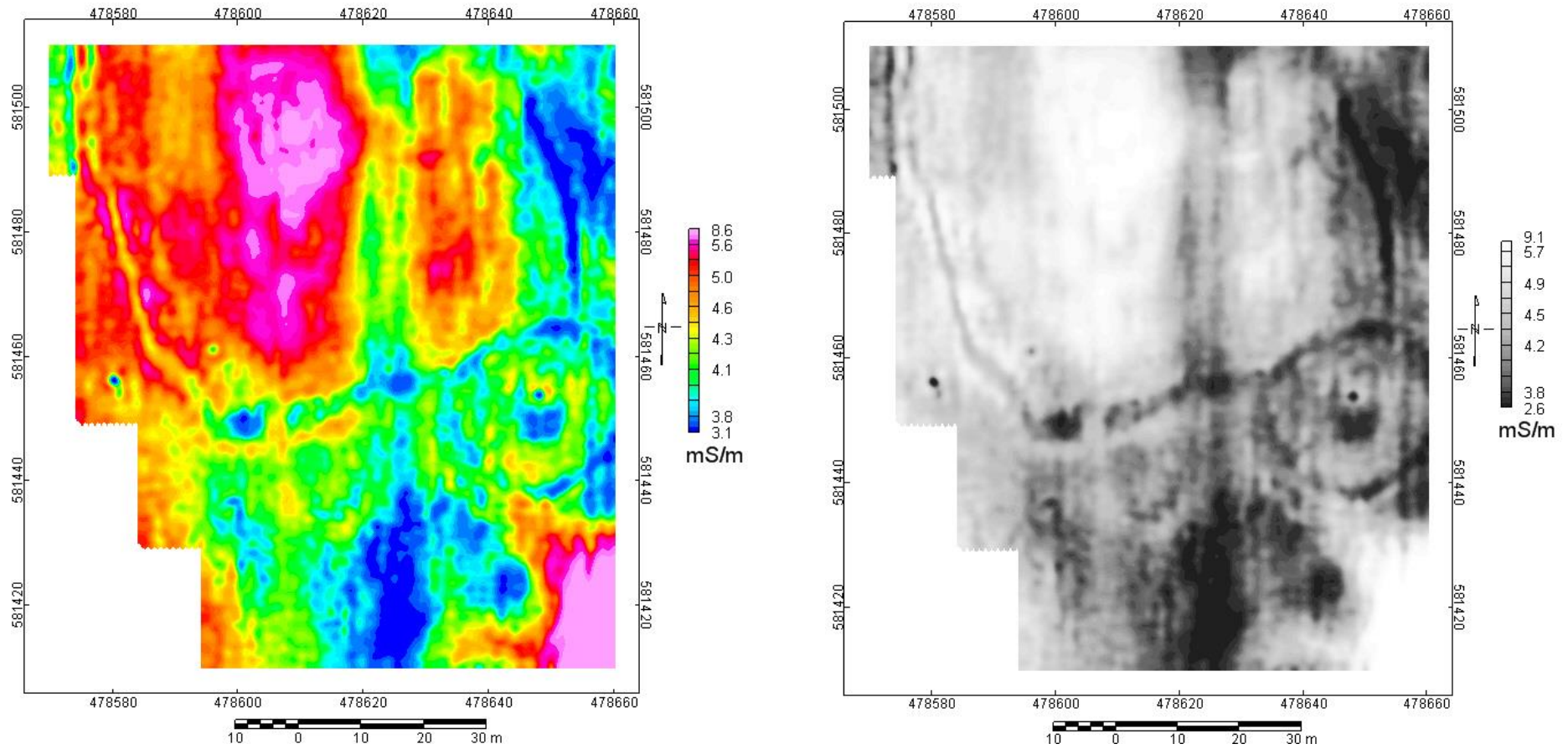


Figure C5. Plots of apparent ground conductivity data and (sensor 1, dipole length = 1.48 m) from survey conducted in 2015.

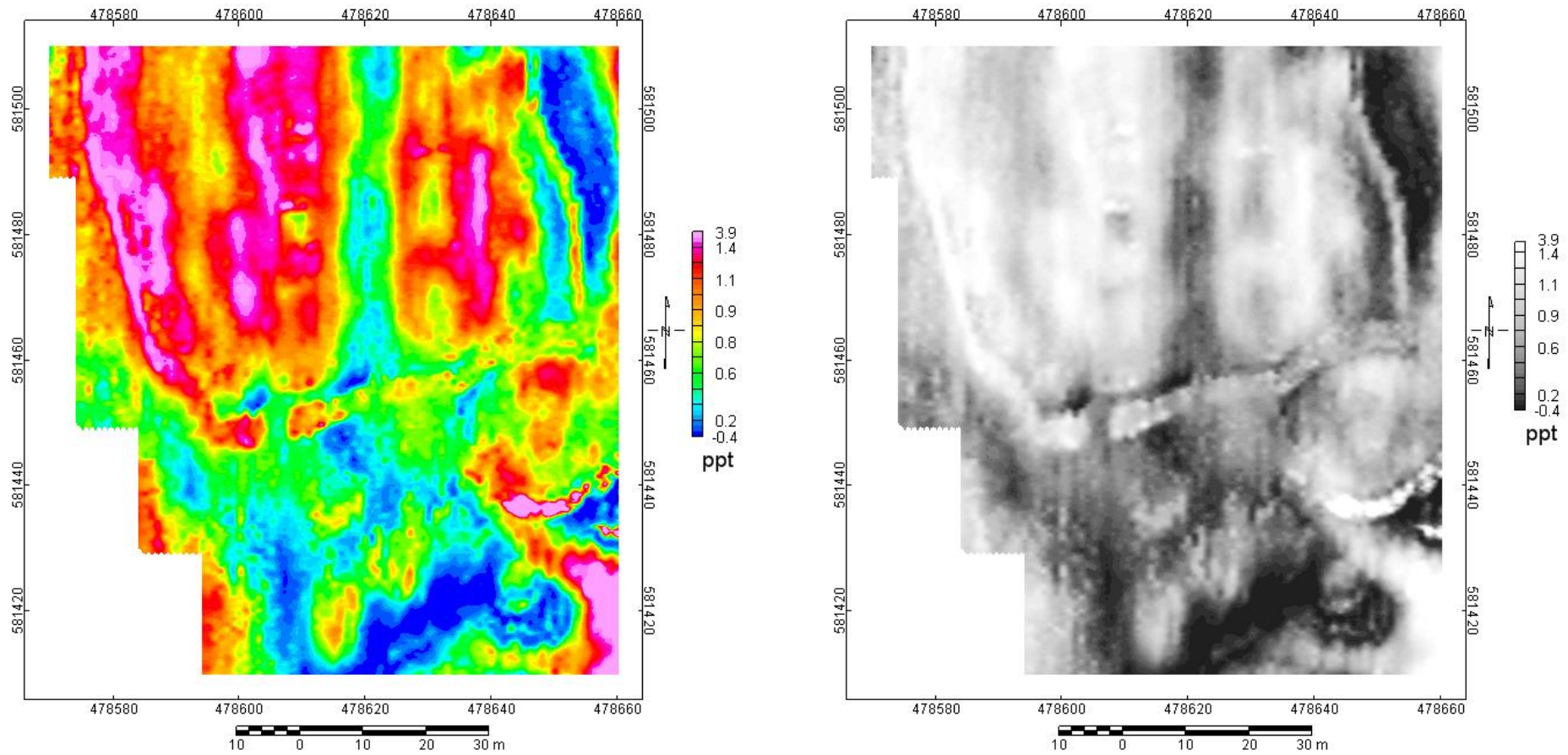


Figure C6. Color Color-contour plot of in-phase data (sensor 1, dipole length = 1.48 m) from survey conducted in 2015. Right: Gray-shaded plot.

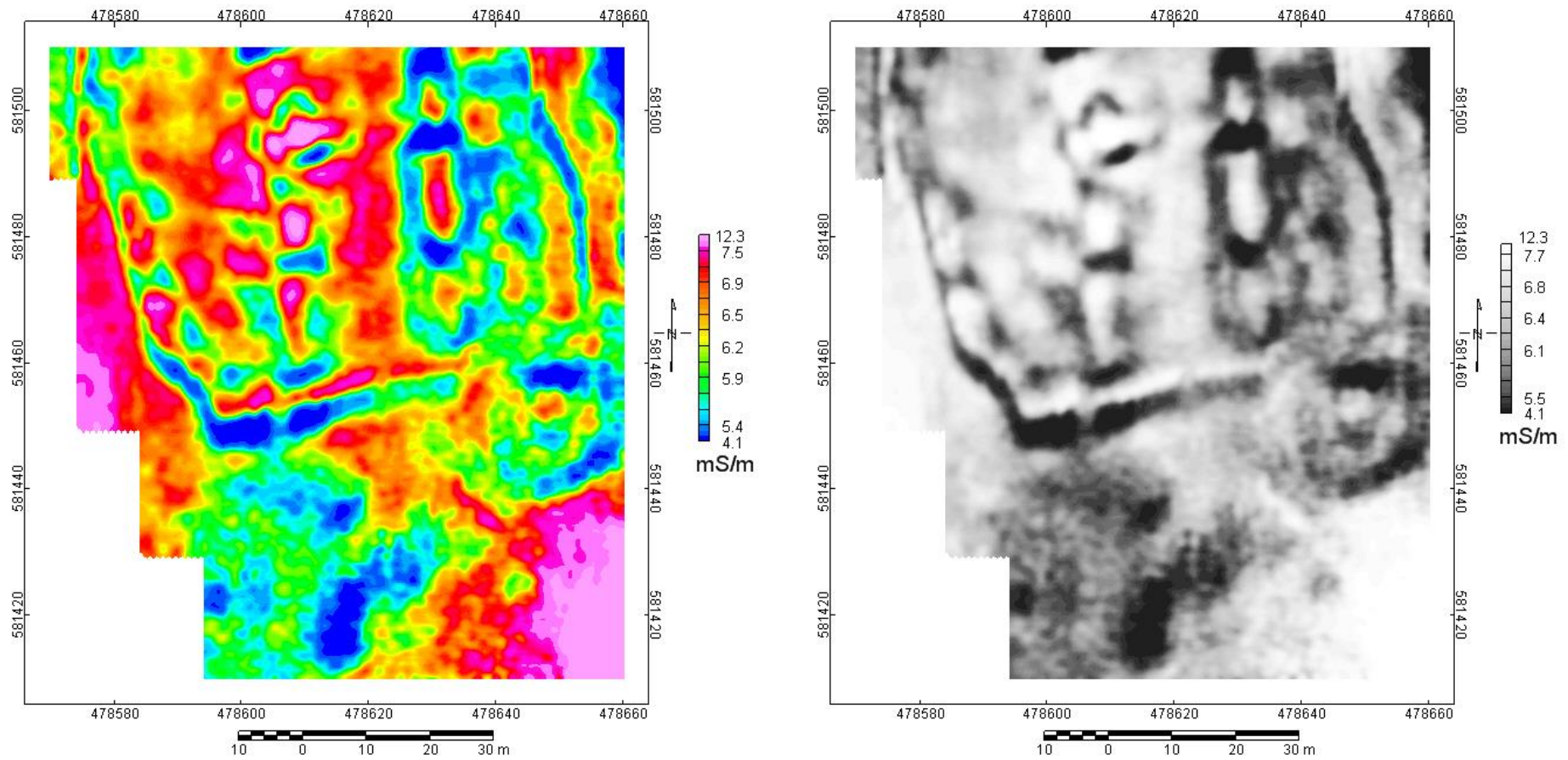


Figure C7. Plots Left: Color-contour plot of apparent ground conductivity data (sensor 3, dipole length = 4.49 m) from survey conducted in 2015. Right: Gray-shaded plot..

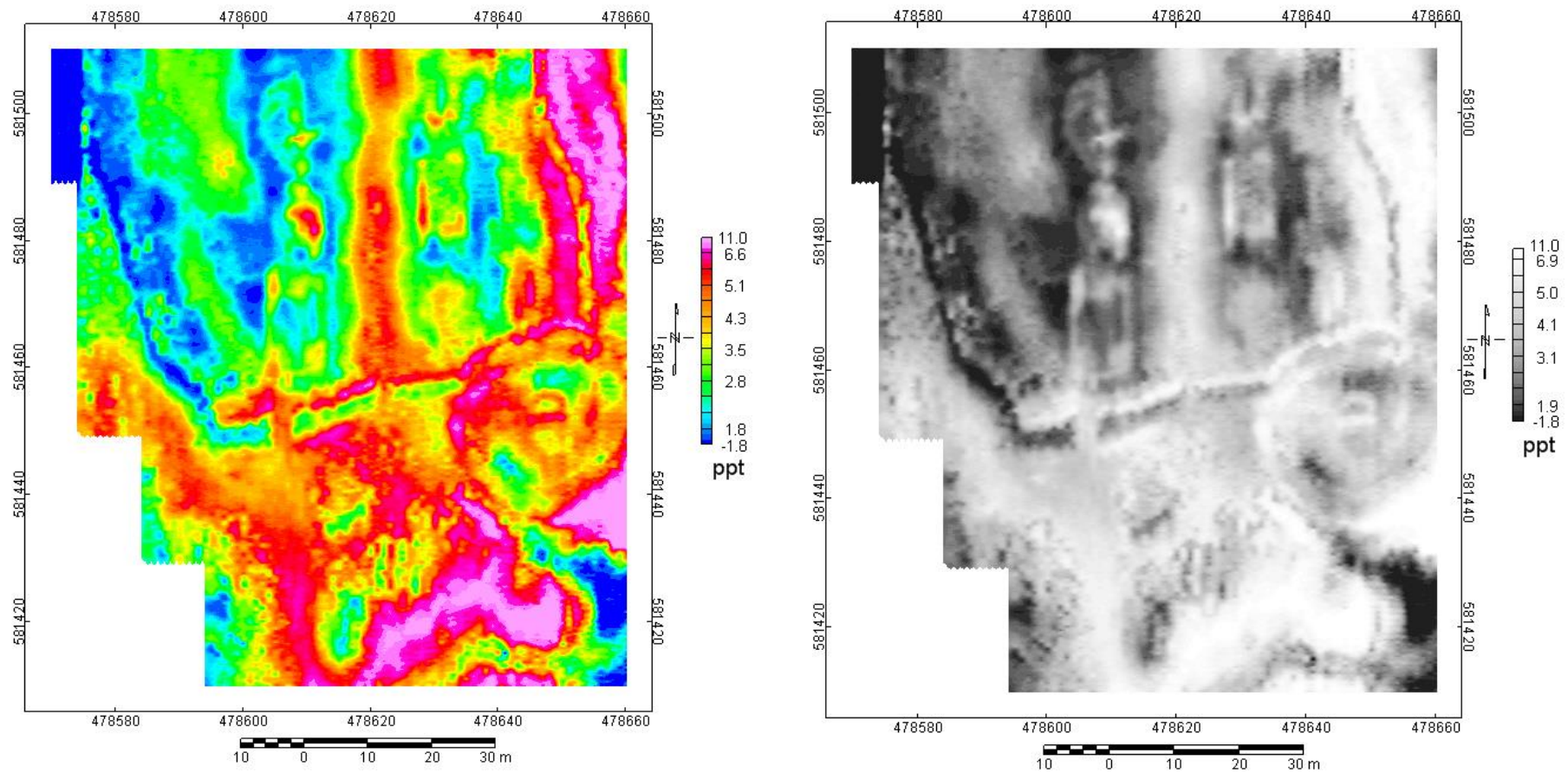


Figure C8. Color-contour plot of in-phase data (sensor 3, dipole length = 4.49 m) from survey conducted in 2015. Right: Gray-shaded plot.

APPENDIX D – ANNOTATED RADARGRAMS

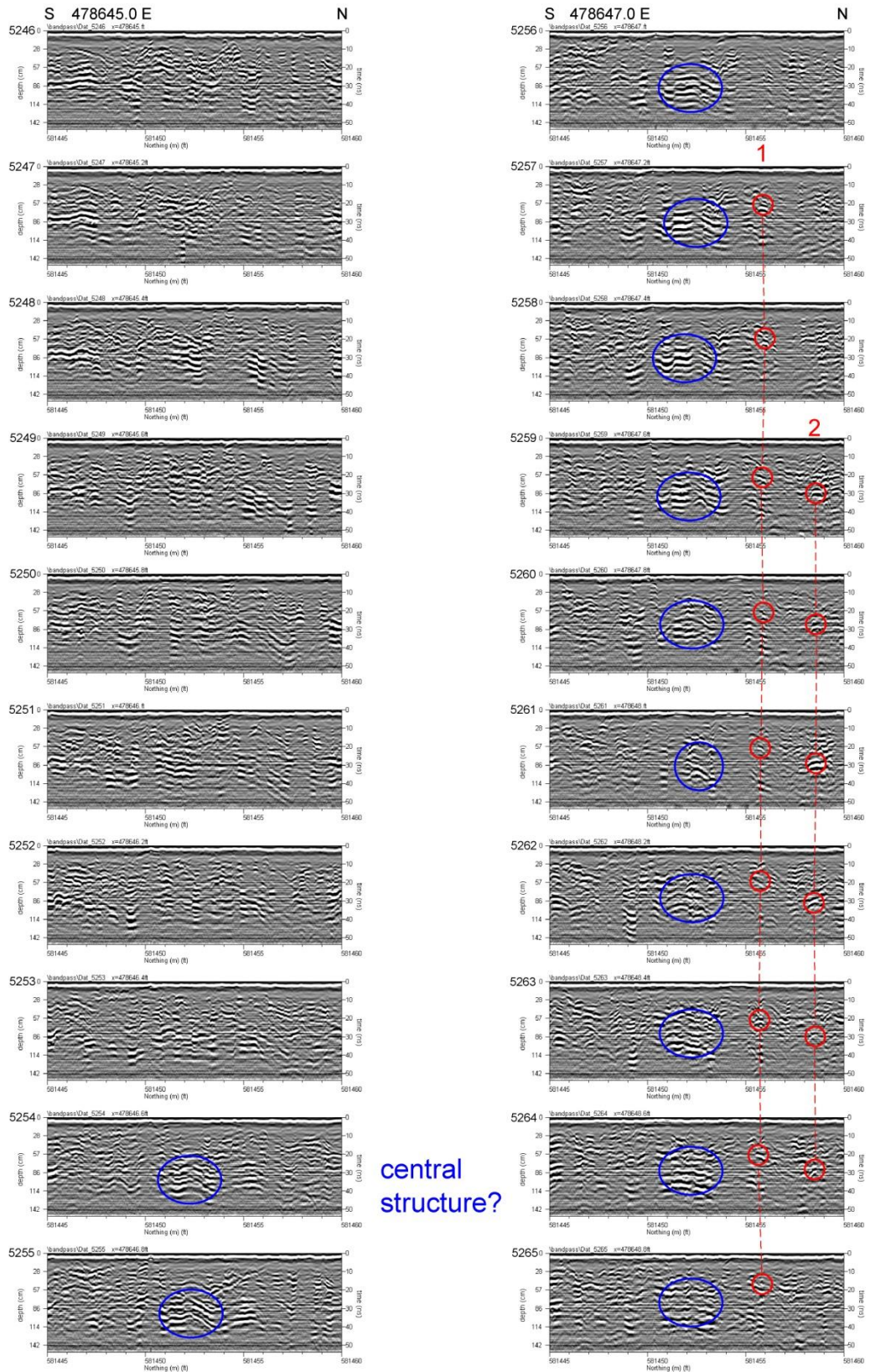


Figure D1. Annotated radargrams for profiles 5246 (478645.0E) through 5265 (478648.8E).

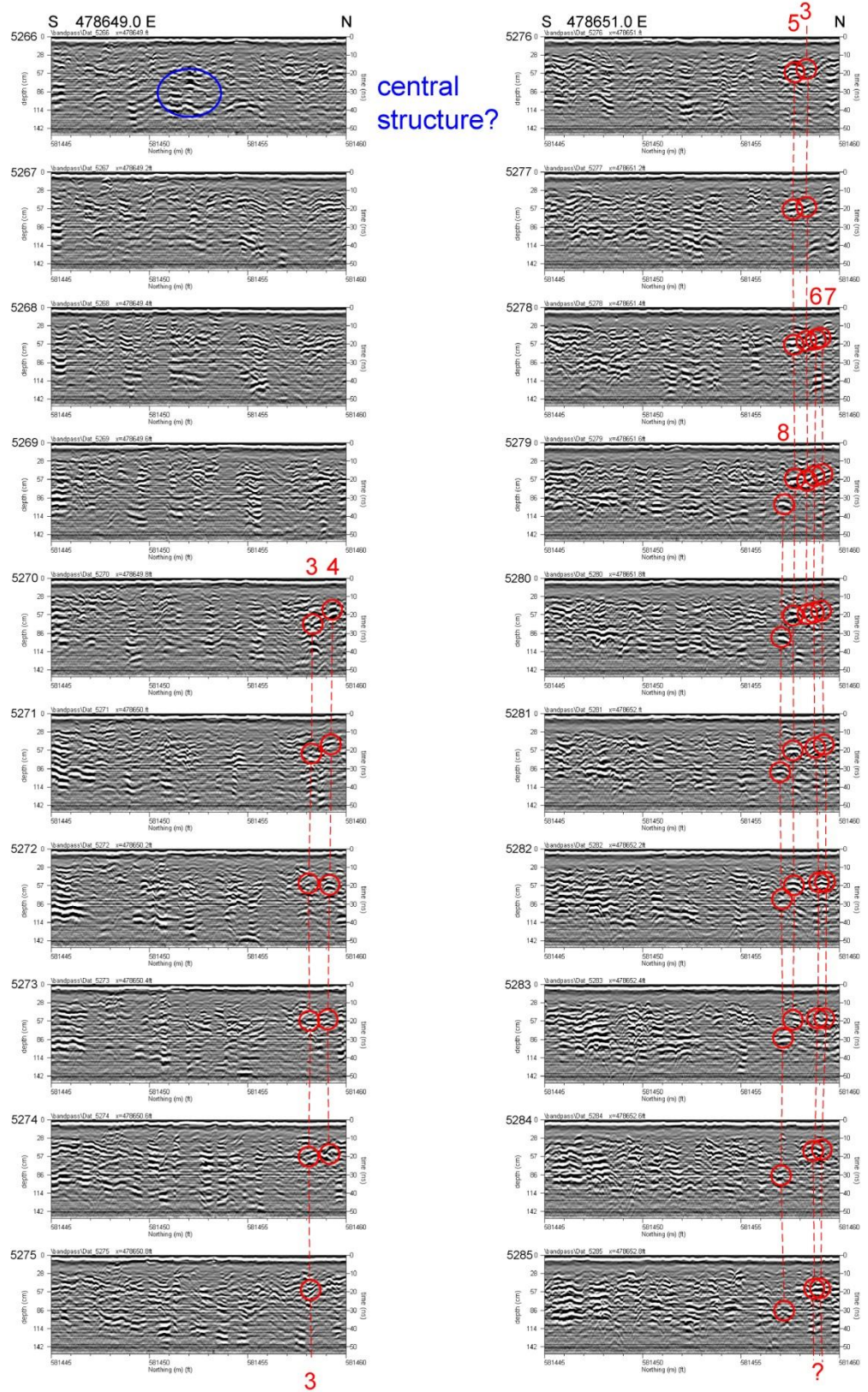


Figure D2. Annotated radargrams for profiles 5266 (478649.0E) through 5285 (478652.8E).

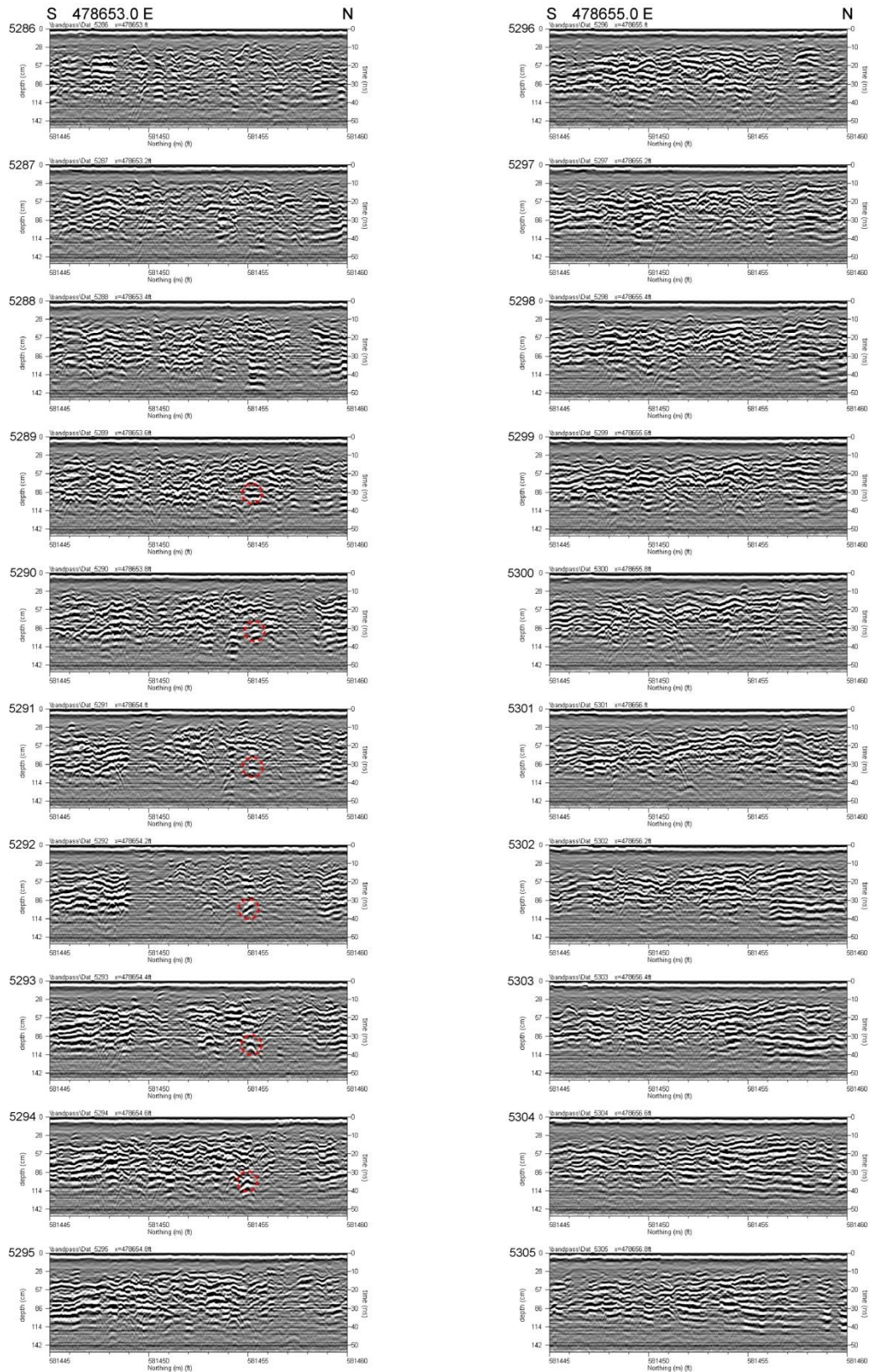


Figure D3. Annotated radargrams for profiles 5286 (478653.0E) through 5305 (478656.8E).

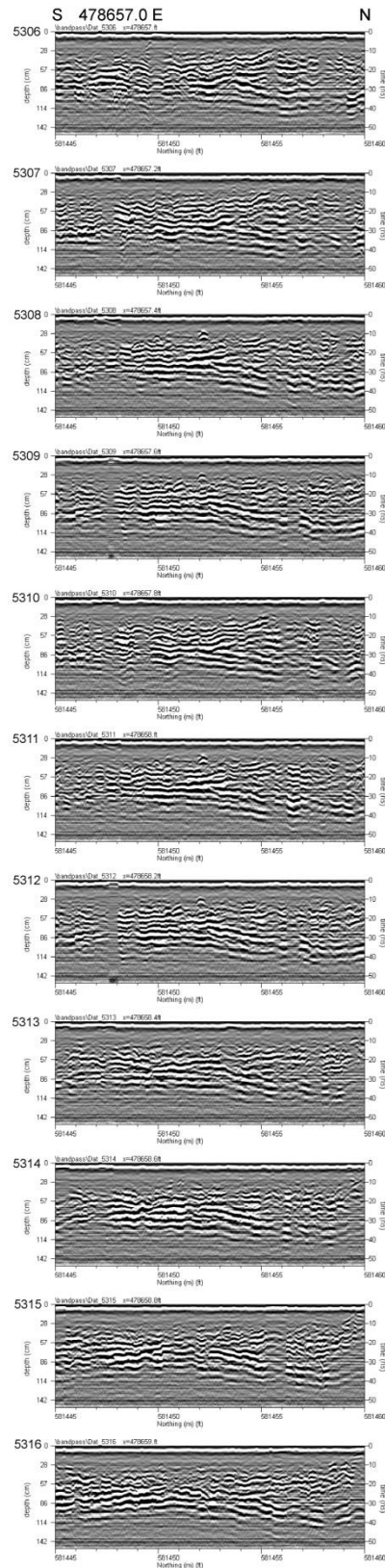
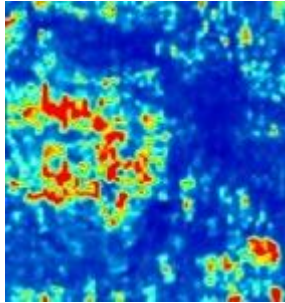
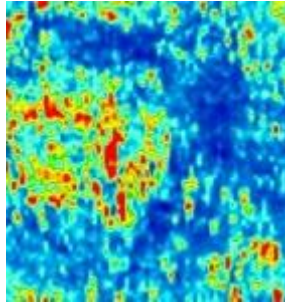


Figure D4. Annotated radargrams for profiles 5306 (478657.0E) through 5316 (478659.0E).

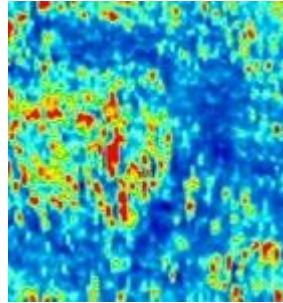
APPENDIX E – GPR SLICES



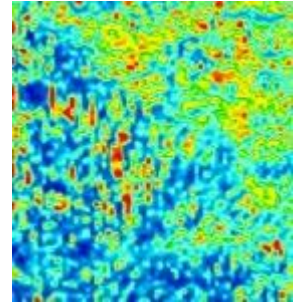
b01(0-8cm)



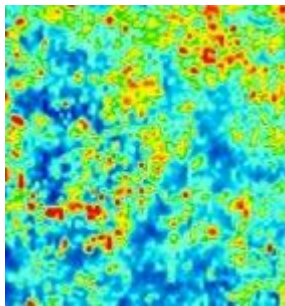
b02(4-12cm)



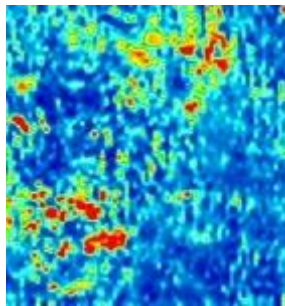
b03(8-16cm)



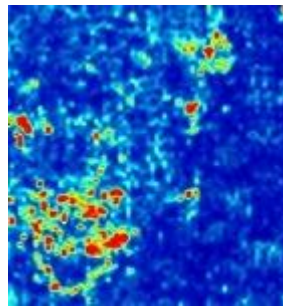
b04(12-20cm)



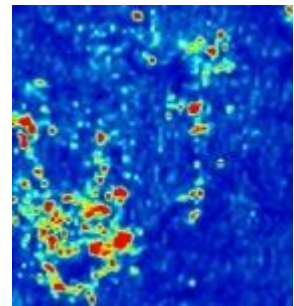
b05(16-23cm)



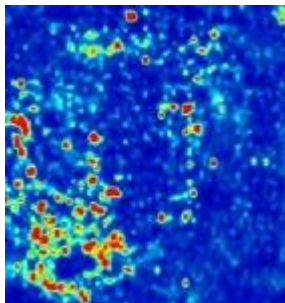
b06(20-27cm)



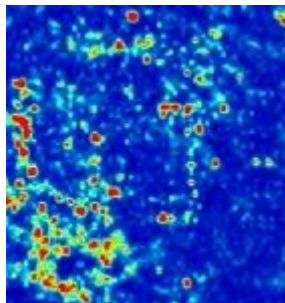
b07(23-31cm)



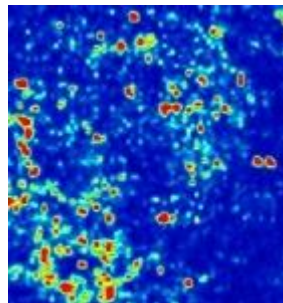
b08(27-35cm)



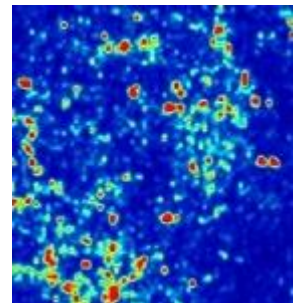
b09(31-39cm)



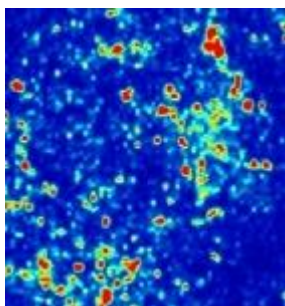
b10(35-43cm)



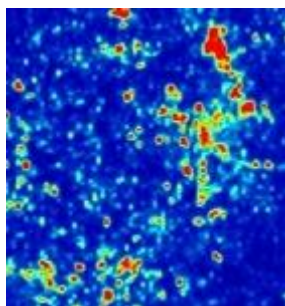
b11(39-47cm)



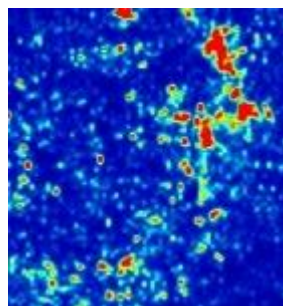
b12(43-51cm)



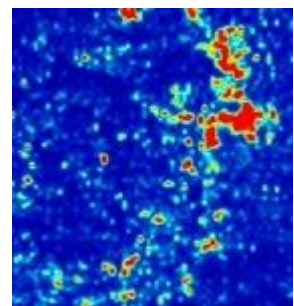
b13(47-55cm)



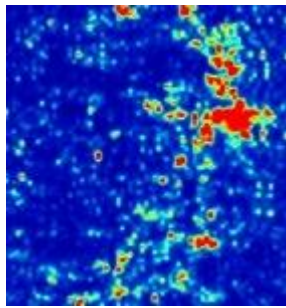
b14(51-59cm)



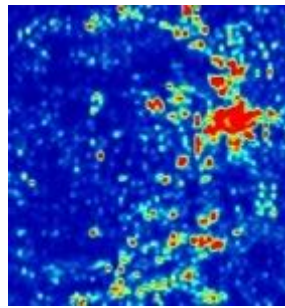
b15(55-63cm)



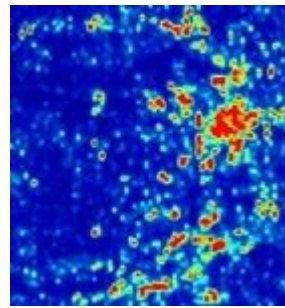
b16(59-67cm)



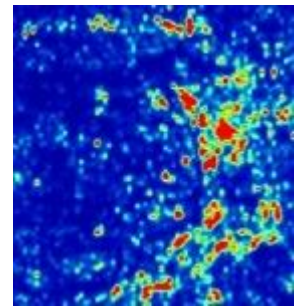
b17(63-71cm)



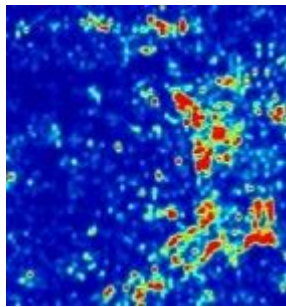
b18(67-75cm)



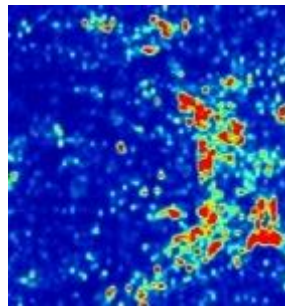
b19(71-79cm)



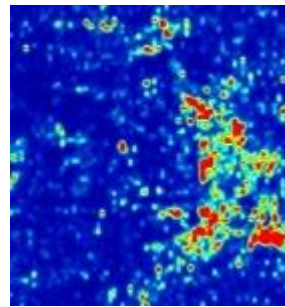
b20(75-82cm)



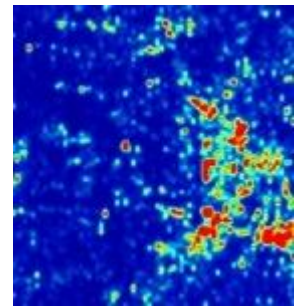
b21(79-86cm)



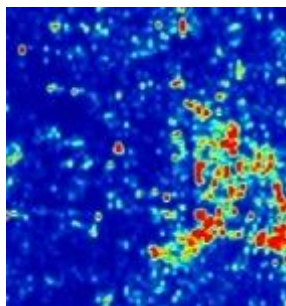
b22(82-90cm)



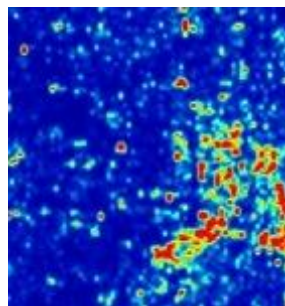
b23(86-94cm)



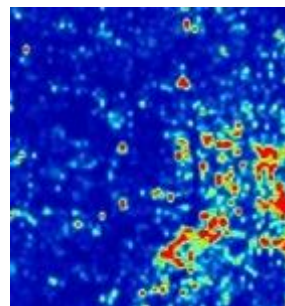
b24(90-98cm)



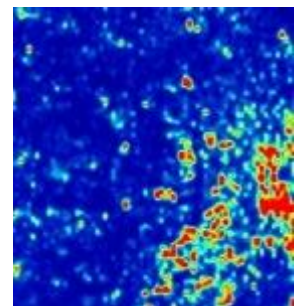
b25(94-102cm)



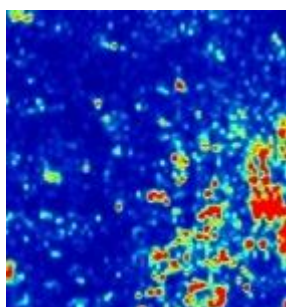
b26(98-106cm)



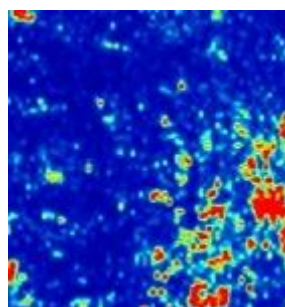
b27(102-110cm)



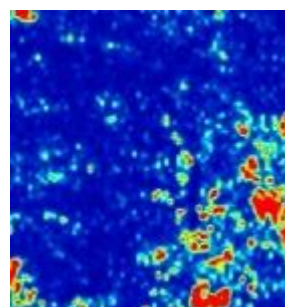
b28(106-114cm)



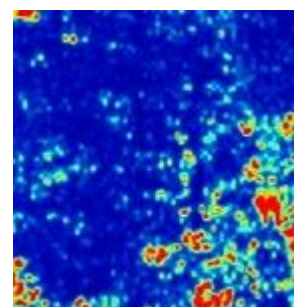
b29(110-118cm)



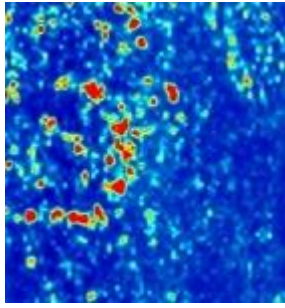
b30(114-121cm)



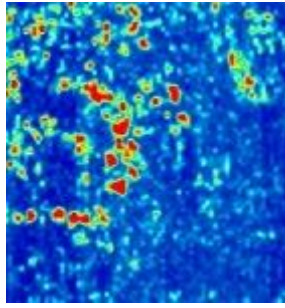
b31(118-126cm)



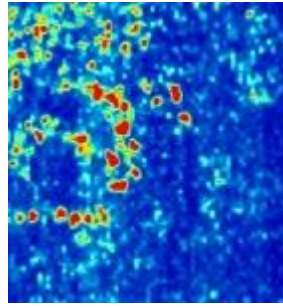
b32(122-130cm)



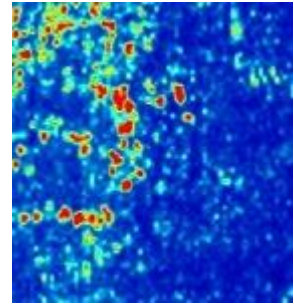
b49(188-196cm)



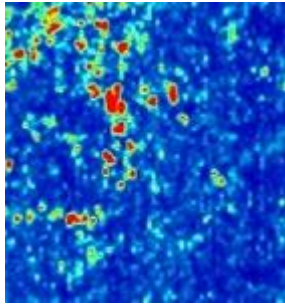
b50(192-200cm)



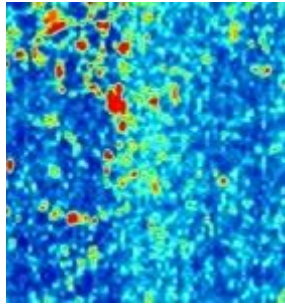
b51(196-204cm)



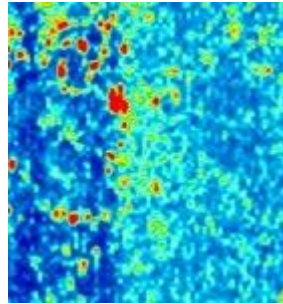
b52(200-208cm)



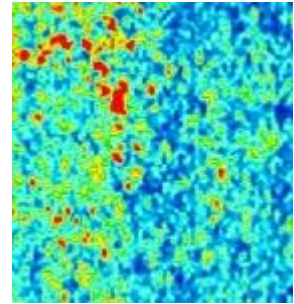
b53(204-212cm)



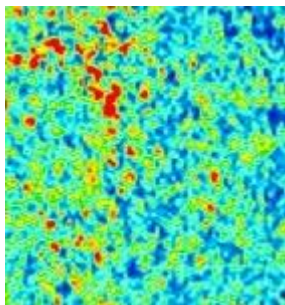
b54(208-216cm)



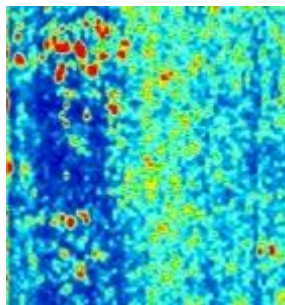
b55(212-220cm)



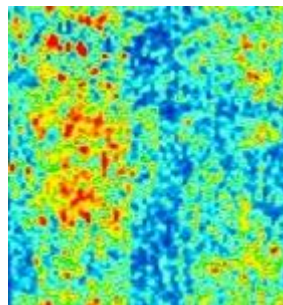
b56(216-224cm)



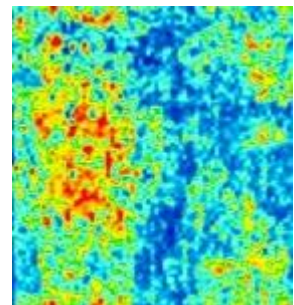
b57(220-228cm)



b58(224-232cm)



b59(228-235cm)



b60(232-235cm)